Discrete unified gas kinetic scheme for flows of binary gas mixture based on the McCormack model

Yue Zhang,[1] Lianhua Zhu,[2] Peng Wang,[2] and Zhaoli Guo[1, a)]

[1)] *State Key Laboratory of Coal Combustion, Huazhong University of Science and Technology, Wuhan 430074, China*

[2)] *James Weir Fluids Laboratory, Department of Mechanical and Aerospace Engineering, University of Strathclyde, Glasgow G1 1XJ, United Kingdom*

(Dated: 30 November 2018)

The discrete unified gas kinetic scheme (DUGKS) was originally developed for single-species flows covering all the regimes, while the gas mixtures are more frequently encountered in engineering applications. Recently, the DUGKS has been extended to binary gas mixtures of Maxwell molecules on the basis of the Andries-Aoki-Perthame kinetic model (AAP) [P. Andries et al., J. Stat. Phys. 106, 993 (2002)]. However, the AAP model cannot recover a correct Prandtl number. In this work, we extend the DUGKS to gas mixture flows based on the McCormack model [F. J. McCormack, Phys. Fluids 16, 2095 (1973)], which can give all the transport coefficients correctly. The proposed method is validated by several standard tests, including the plane Couette flow, the Fourier flow, and the lid-driven cavity flow under different mass ratios and molar concentrations. Good agreement between results of the DUGKS and the other well-established numerical methods shows that the proposed DUGKS is effective and reliable for binary gas mixtures in all flow regimes. In addition, the DUGKS is about two orders of magnitude faster than the DSMC for low-speed flows in terms of the wall time and convergent iteration steps.

Keywords: binary gas mixtures, McCormack model, kinetic scheme, rarefied gas dynamics

[a)] Electronic mail: Corresponding author: zlguo@hust.edu.cn

I. INTRODUCTION

Gas mixture flows are frequently encountered in engineering applications, such as the Micro-Electro-Mechanical-Systems (MEMS), solid oxide fuel cells and vacuum technologies. Flows in those fields usually involve a wide range of Knudsen number (Kn), which is defined as the ratio of the mean free path of molecules to the characteristic length. The difficulties arise for flows in the transition ($0.1 \lesssim \mathrm{Kn} \lesssim 10$) and free-molecular ($\mathrm{Kn} \gtrsim 10$) regimes, in which the traditional hydrodynamic equations such as the Navier-Stokes equations fail to describe the non-equilibrium effects due to the gas rarefaction of gas mixture flows[1].

As well known, the multi-species Boltzmann equation is able to accurately describe gas mixture flows in all regimes. However, solving the Boltzmann equation is difficult analytically. The direct simulation Monte Carlo (DSMC) method is a prevailing numerical technique for solving the Boltzmann equation for high-speed flows in the transition and free-molecule regimes[2–6]. While the statistical noise appearing in DSMC makes it unsuitable for low-speed and unsteady flows. In addition, the computational costs of the DSMC method are expensive in the near-continuum regime ($\mathrm{Kn} \lesssim 0.01$), as the cell size and time step in the DSMC are limited by the mean free path and the collision time of molecules, respectively. Recently, some improvements have been made to ease the difficulties[7–10]. It is noted that the deterministic Boltzmann solvers can also be applied to gas mixture flows in simple geometries by direct discretizing the full Boltzmann equation[11–15]. Although accurate results can be obtained by these deterministic methods, they are generally very complicated and computationally expensive.

As a consequence, great efforts have been devoted to developing Boltzmann model equations for gas mixtures by simplifying the collision term and retaining the physical properties of the original collision term as much as possible. Similar to the Bhatnagar-Gross-Krook (BGK)[16] model for the single species, several BGK-type collision operators for gas mixtures have been proposed[17–20]. In this type of model equations, the self-collision and cross-collision effects are included in a single or multiple relaxation time operators. However, the agreement between results of the Boltzmann equation and the BGK-type model for gas mixtures is difficult to achieve, since additional physical effects are brought about by cross collisions. Most of the existing BGK-type models are not able to give the transport coefficients accurately, except the McCormack model[21] which linearizes the collision term with the assumption that

the system slightly deviates from the equilibrium due to small perturbations. The moments of the collision term of the McCormack model approximate the Boltzmann equation up to the third order, and therefore the McCormack model can reproduce all transport coefficients correctly. Owing to this advantage, the McCormack model has been widely applied to gas mixture flows[22–27].

Based on model equations, several types of kinetic method have already been developed for gas mixture flows, such as the lattice Boltzmann method[28,29], the discrete velocity methods (DVM)[30,31], and the analytical version of the discrete ordinate method[32,33]. Besides, the unified gas kinetic scheme (UGKS) for binary gas mixtures of hard sphere molecules has been developed based on the Andries-Aoki-Perthame (AAP) kinetic model[34,35].

Recently, the discrete unified gas kinetic scheme (DUGKS)[36,37] was developed for single-species flows covering a wide flow regimes. With the coupling of particle transport and collision effects, the DUGKS exhibits the nice asymptotic preserving (AP) property[38,39] thus is suitable for different flow regimes. The DUGKS has already been applied successfully to complex flows of single-species gases from continuum to rarefied regimes[40–45]. Very recently, the DUGKS was extended to gas mixture flows of Maxwell molecules based on the AAP model[46]. However, due to the limitation of the AAP model, the DUGKS can only recover one transport coefficient correctly[46].

The aim of this work is to further develop the DUGKS for binary gas mixtures based on the McCormack model, such that the correct transport coefficients can be fully achieved. The remaining of this paper is organized as follows. In Sec. II, the McCormack model for binary gas mixtures will be introduced. Then the DUGKS for gas mixtures will be constructed on the basis of the McCormack model in Sec. III. Several numerical tests are performed in Sec. IV to validate the proposed method, followed by a summary in Sec. V.

II. THE MCCORMACK MODEL FOR GAS MIXTURES

The Boltzmann equation for a binary gas mixture with species A and B can be written as[47],

$$\frac{\partial f_\alpha}{\partial t'} + \boldsymbol{\xi} \cdot \boldsymbol{\nabla} f_\alpha = Q_\alpha(f, f), \tag{1}$$

where

$$Q_\alpha(f,f)=\sum_{\alpha=A,B}Q_{\alpha\beta}(f_\alpha,f_\beta),\quad Q_{\alpha\beta}(f_\alpha,f_\beta)=\int_{R^3}\int_{B_+}(f'_\alpha f'_{\beta^*}-f_\alpha f_{\beta^*})B_{\alpha\beta}(\boldsymbol{N}\cdot\boldsymbol{V},|\boldsymbol{V}|)d\boldsymbol{\xi}_*d\boldsymbol{N}. \tag{2}$$

In the above equation, the Greek letters α and β denote symbolically the gas species; $f_\alpha \equiv f_\alpha(\boldsymbol{x},\boldsymbol{\xi},t)$ represents the distribution function of species α with particle velocity $\boldsymbol{\xi}$ at position $\boldsymbol{x}$ and time t in three-dimensional physical space; $Q_\alpha(f,f)$ is the Boltzmann collision operator for species α with $B_{\alpha\beta}(\boldsymbol{N}\cdot\boldsymbol{V},|\boldsymbol{V}|)$ being the collision kernel depending on the intermolecular force between species α and β; $\boldsymbol{\xi}$ and $\boldsymbol{\xi_*}$ are pre-collision velocities, $\boldsymbol{N}$ is a unit vector and B_+ is the semi-sphere defined by $\boldsymbol{N}\cdot\boldsymbol{V}=0$, where $\boldsymbol{V}=\boldsymbol{\xi}-\boldsymbol{\xi}_*$ is the relative velocity. According to the conservation laws of momentum and energy:

$$\begin{cases} m_\alpha\boldsymbol{\xi}+m_\beta\boldsymbol{\xi}_*=m_\alpha\boldsymbol{\xi}'+m_\beta\boldsymbol{\xi}'_*, \\ m_\alpha|\xi|^2+m_\beta|\xi_*|^2=m_\alpha|\xi'|^2+m_|\xi'_*|^2, \end{cases} \tag{3}$$

the post-collision velocities $\boldsymbol{\xi}'$ and $\boldsymbol{\xi}'_*$ can be written as

$$\begin{cases} \boldsymbol{\xi}'=\boldsymbol{\xi}-\frac{2m_{\alpha\beta}}{m_\alpha}\boldsymbol{N}[(\boldsymbol{\xi}-\boldsymbol{\xi}_*)\cdot\boldsymbol{N}], \\ \boldsymbol{\xi}'_*=\boldsymbol{\xi}_*+\frac{2m_{\alpha\beta}}{m_\beta}\boldsymbol{N}[(\boldsymbol{\xi}-\boldsymbol{\xi}_*)\cdot\boldsymbol{N}], \end{cases} \tag{4}$$

where $m_{\alpha\beta}$ is the reduced mass, which can be expressed in terms of the mass of species m_α as

$$m_{\alpha\beta}=\frac{m_\alpha m_\beta}{(m_\alpha+m_\beta)}. \tag{5}$$

Without loss of generality, we assume $m_A<m_B$.

For systems slightly deviate from equilibrium caused by small perturbations, the McCormack model linearizes the full Boltzmann equation (1) by equaling the moments of the third-order linearized collision operator to those of the full collision operator. As the concentration, pressure or temperature gradients are sufficiently small, the distribution function of species α can be linearized as $f_\alpha=f_\alpha^M(\boldsymbol{\xi})(1+h_\alpha\epsilon)$, where ϵ is far smaller than 1, f_α^M is the absolute Maxwellian equilibrium distribution function written in terms of the constant density $n_{0\alpha}$ and temperature T_0

$$f_\alpha^M(\boldsymbol{\xi})=n_{0\alpha}\left(\frac{m_\alpha}{2\pi k_BT_0}\right)^{3/2}\exp\left[-\frac{m_\alpha\xi^2}{2k_BT_0}\right], \tag{6}$$

where k_B is the Boltzmann constant and h_α is the perturbation distribution function. Then the linearized Boltzmann equation can be expressed as

$$\frac{\partial h_\alpha}{\partial t'} + \boldsymbol{\xi} \cdot \frac{\partial h_\alpha}{\partial \boldsymbol{x}'} = \sum_{\beta=A,B} L_{\alpha\beta} h, \quad \alpha = A, B, \tag{7}$$

where $L_{\alpha\beta}h$ is the linearized Boltzmann collision operator. It is noted that we only solve the governing equation for h_α in Eq. (7) instead that of f_α in the present work. Therefore the value of ϵ is irrelevant to the evolution of distribution function h_α. Previous work[4,5] have demonstrated that the equation $f_\alpha = f_\alpha^M(\boldsymbol{\xi})(1 + h_\alpha \epsilon)$ can be satisfied with $\epsilon = 0.2$.

Furthermore, the deviated macroscopic quantities of species α from equilibrium values, such as the deviated molecular number density n'_α, flow velocity $\boldsymbol{u}'_\alpha$, shear stress $P'_{\alpha ik}(i, k = x, y, z)$, temperature T'_α, and heat flux $\boldsymbol{q}'_\alpha$ can be calculated from the moments of h_α. For convenience, we introduce the following dimensionless quantities:

$$\begin{aligned} &\boldsymbol{x} = \frac{\boldsymbol{x}'}{H}, \quad \boldsymbol{c}_\alpha = \sqrt{\frac{m_\alpha}{2k_B T_0}}\boldsymbol{\xi}, \quad t = \frac{t'}{H/v_0}, \quad n_\alpha = \frac{n'}{n_{0\alpha}\epsilon}, \\ &\boldsymbol{u}_\alpha = \frac{\boldsymbol{u}'_\alpha}{U}, \quad P_{\alpha xy} = -\frac{P'_{\alpha xy}}{2p_{0\alpha}\epsilon}, \quad T_\alpha = \frac{T'_\alpha}{T_0\epsilon}, \quad \boldsymbol{q}_\alpha = \frac{\boldsymbol{q}'_\alpha}{p_{0\alpha}v_0\epsilon}, \end{aligned} \tag{8}$$

where H is the characteristic length, U is characteristic speed, $p_{0\alpha} = n_{0\alpha}k_B T_0$ is the partial pressure of the species α, and $v_0 = \sqrt{m/2k_B T_0}$ is the molecular velocity of the mixture with $m = C_0 m_A + (1 - C_0)m_B$ being the mean molecular mass of the mixture and $C_0 = n_{0A}/(n_{0A} + n_{0B})$ the equilibrium molar concentration of the light species.

Then the dimensionless governing equation of species α can be obtained

$$\frac{\partial h_\alpha}{\partial t} + \hat{\boldsymbol{c}}_\alpha \cdot \frac{\partial h_\alpha}{\partial \boldsymbol{x}} = H\sqrt{\frac{m}{2k_B T_0}} \sum_{\beta=A,B} L_{\alpha\beta} h = H\sqrt{\frac{m}{2k_B T_0}} L_\alpha h, \quad \alpha = A, B, \tag{9}$$

where $\hat{\boldsymbol{c}}_\alpha = \sqrt{m/m_\alpha}\boldsymbol{c}_\alpha$ and the linearized collision operator $L_{\alpha\beta}h$ of the McCormack model is given as

$$\begin{aligned} L_{\alpha\beta}h = &-\gamma_{\alpha\beta}h_\alpha + \gamma_{\alpha\beta}n_\alpha \\ &+ 2\sqrt{\frac{m_\alpha}{m}}\left[\gamma_{\alpha\beta}u_{\alpha i} - \nu^{(1)}_{\alpha\beta}(u_{\alpha i} - u_{\beta i}) - \nu^{(2)}_{\alpha\beta}(q_{\alpha i} - \frac{m_\alpha}{m_\beta}q_{\beta i})\right] c_{\alpha i} \\ &+ \left[\gamma_{\alpha\beta}T_\alpha - 2\frac{m_{\alpha\beta}}{m_\beta}(T_\alpha - T_\beta)\nu^{(1)}_{\alpha\beta}\right]\left(c_\alpha^2 - \frac{3}{2}\right) \\ &+ 2\left[(\gamma_{\alpha\beta} - \nu^{(3)}_{\alpha\beta})P_{\alpha ik} + \nu^{(4)}_{\alpha\beta}P_{\beta ik}\right] c_{\alpha i}c_{\alpha k} \\ &+ \frac{8}{5}\sqrt{\frac{m_\alpha}{m}}\left[(\gamma_{\alpha\beta} - \nu^{(5)}_{\alpha\beta})q_{\alpha i} + \nu^{(6)}_{\alpha\beta}\sqrt{\frac{m_\beta}{m_\alpha}}q_{\beta i} - \frac{5}{8}\nu^{(2)}_{\alpha\beta}(u_{\alpha i} - u_{\beta i})\right] c_{\alpha i}\left(c_\alpha^2 - \frac{5}{2}\right), \end{aligned} \tag{10}$$

where the quantities $\nu_{\alpha\beta}^{(n)}$ are given by

$$\nu_{\alpha\beta}^{(1)} = \frac{16}{3}\frac{m_{\alpha\beta}}{m_\alpha} n_\beta \Omega_{\alpha\beta}^{11}, \tag{11a}$$

$$\nu_{\alpha\beta}^{(2)} = \frac{64}{15}\left(\frac{m_{\alpha\beta}}{m_\alpha}\right)^2 n_\beta \left[\Omega_{\alpha\beta}^{12} - \frac{5}{2}\Omega_{\alpha\beta}^{11}\right], \tag{11b}$$

$$\nu_{\alpha\beta}^{(3)} = \frac{16}{5}\frac{m_{\alpha\beta}^2}{m_\alpha m_\beta} n_\beta \left[\frac{10}{3}\Omega_{\alpha\beta}^{11} + \frac{m_\beta}{m_\alpha}\Omega_{\alpha\beta}^{22}\right], \tag{11c}$$

$$\nu_{\alpha\beta}^{(4)} = \frac{16}{5}\frac{m_{\alpha\beta}^2}{m_\alpha m_\beta} n_\beta \left[\frac{10}{3}\Omega_{\alpha\beta}^{11} - \Omega_{\alpha\beta}^{22}\right], \tag{11d}$$

$$\nu_{\alpha\beta}^{(5)} = \frac{64}{15}\left(\frac{m_{\alpha\beta}}{m_\alpha}\right)^3 \frac{m_\alpha}{m_\beta} n_\beta \left[\Omega_{\alpha\beta}^{22} + \left(\frac{15}{4}\frac{m_\alpha}{m_\beta} + \frac{25}{8}\frac{m_\beta}{m_\alpha}\right)\Omega_{\alpha\beta}^{11} - \frac{1}{2}\frac{m_\beta}{m_\alpha}\left(5\Omega_{\alpha\beta}^{12} - \Omega_{\alpha\beta}^{13}\right)\right], \tag{11e}$$

$$\nu_{\alpha\beta}^{(5)} = \frac{64}{15}\left(\frac{m_{\alpha\beta}}{m_\alpha}\right)^3 \left(\frac{m_\alpha}{m_\beta}\right)^{3/2} n_\beta \left[-\Omega_{\alpha\beta}^{22} + \frac{55}{8}\Omega_{\alpha\beta}^{11} - \frac{5}{2}\Omega_{\alpha\beta}^{12} + \frac{1}{2}\Omega_{\alpha\beta}^{13}\right], \tag{11f}$$

where $\Omega_{\alpha\beta}^{\sigma\eta}$ is the omega integral[48], which depends on the intermolecular potential. For the hard sphere model, it is defined by[48]

$$\Omega_{\alpha\beta}^{\sigma\eta} = \frac{(\eta+1)!}{8}\left[1 - \frac{1+(-1)^\sigma}{2(\sigma+1)}\right]\left(\frac{\pi k_B T}{2m_{\alpha\beta}}\right)^{1/2}(d_\alpha + d_\beta)^2, \tag{12}$$

where d_α is the molecular diameter of species α. In Eq. (11), the parameter $\gamma_{\alpha\beta}$ is proportional to the collision frequency between species α and β and appears only in the form of combinations

$$\gamma_A = \gamma_{AA} + \gamma_{AB}, \quad \gamma_B = \gamma_{BB} + \gamma_{BA}. \tag{13}$$

So it is convenient to define γ_A and γ_B only, which can be related to the viscosity in the same formation with that of the Shakhov model[22,49,50]

$$\gamma_\alpha = \frac{p_{0\alpha}}{\mu_\alpha}, \tag{14}$$

where μ_α is the partial viscosity given as

$$\mu_\alpha = p_{0\alpha}\frac{S_\beta + \nu_{\alpha\beta}^{(4)}}{S_\alpha S_\beta - \nu_{\alpha\beta}^{(4)}\nu_{\beta\alpha}^{(4)}}, \quad S_\alpha = \nu_{\alpha\alpha}^{(3)} - \nu_{\alpha\alpha}^{(4)} + \nu_{\alpha\beta}^{(3)}, \quad \beta \neq \alpha. \tag{15}$$

The viscosity of the mixture is given by

$$\mu = \mu_A + \mu_B. \tag{16}$$

Once the perturbation distribution function h_α is known, the deviated quantities can be calculated as

$$n_\alpha = \int f_\alpha^0 h_\alpha d\boldsymbol{c}_\alpha, \tag{17a}$$

$$\boldsymbol{u}_\alpha = \sqrt{\frac{m}{m_\alpha}} \int \boldsymbol{c}_\alpha f_\alpha^0 h_\alpha d\boldsymbol{c}_\alpha, \tag{17b}$$

$$P_{\alpha ik} = \int \left(c_{\alpha i} c_{\alpha k} - \frac{1}{3} c_\alpha^2 \delta_{ik} \right) f_\alpha^0 h_\alpha d\boldsymbol{c}_\alpha, \tag{17c}$$

$$T_\alpha = \int \left(\frac{2}{3} c_\alpha^2 - 1 \right) f_\alpha^0 h_\alpha d\boldsymbol{c}_\alpha, \tag{17d}$$

$$\boldsymbol{q}_\alpha = \frac{1}{2} \sqrt{\frac{m}{m_\alpha}} \int \boldsymbol{c}_\alpha \left(c_\alpha^2 - \frac{5}{2} \right) f_\alpha^0 h_\alpha d\boldsymbol{c}_\alpha, \tag{17e}$$

where $f_\alpha^0 = \pi^{-3/2} \exp(-c_\alpha^2)$. The deviated quantities of the mixture are then determined by

$$n(\boldsymbol{x}) = \frac{n'_A + n'_B}{n_0 \epsilon} = C_0 n_A(\boldsymbol{x}) + (1 - C_0) n_B(\boldsymbol{x}), \tag{18a}$$

$$\boldsymbol{u}(\boldsymbol{x}) = \frac{m_A n_{0A} \boldsymbol{u}'_A + m_B n_{0B} \boldsymbol{u}'_B}{n_0 m U} = \frac{C_0 m_A \boldsymbol{u}_A(\boldsymbol{x}) + (1 - C_0) m_B \boldsymbol{u}_B(\boldsymbol{x})}{m}, \tag{18b}$$

$$P_{ik}(\boldsymbol{x}) = \frac{P'_{Aik} + P'_{Bik}}{2 p_0 \epsilon} = C_0 P_{Aik}(\boldsymbol{x}) + (1 - C_0) P_{Bik}(\boldsymbol{x}), \tag{18c}$$

$$T(\boldsymbol{x}) = \frac{n_{0A} T'_A + n_{0B} T'_B}{n_0 \epsilon} = C_0 T_A(\boldsymbol{x}) + (1 - C_0) T_B(\boldsymbol{x}), \tag{18d}$$

$$\boldsymbol{q}(\boldsymbol{x}) = \frac{\boldsymbol{q}'_A + \boldsymbol{q}'_B}{p_0 v_0 \epsilon} = C_0 \boldsymbol{q}_A(\boldsymbol{x}) + (1 - C_0) \boldsymbol{q}_B(\boldsymbol{x}), \tag{18e}$$

where $p_0 = n_0 k_B T_0$ and $n_0 = n_{0A} + n_{0B}$ are the pressure and number density of the mixture, respectively.

For D (< 3) dimensional problems, the kinetic equation (9) can be simplified by introducing reduced distribution functions. Specially, the perturbation distribution function h_α can be expressed as $h_\alpha = h_\alpha(\boldsymbol{x}, \boldsymbol{c}_\alpha, \boldsymbol{\eta}_\alpha, t)$, where $\boldsymbol{x} = (x_1, \ldots, x_D)$ and $\boldsymbol{c_\alpha} = (c_{\alpha 1}, \ldots, c_{\alpha D})$. In addition, $\boldsymbol{\eta}_\alpha = (c_{\alpha(D+1)}, \ldots, c_{\alpha 3})$ is a vector of length $L = 3 - D$, consisting of the rest components of the three-dimensional velocity space $(c_{\alpha 1}, c_{\alpha 2}, c_{\alpha 3})$. Since the evolution of the perturbation distribution function h_α depends only on the D-dimensional velocity and is irrelevant to $\boldsymbol{\eta}_\alpha$, two reduced distribution functions are used to remove the dependence of the passive variable[51,52]

$$g_\alpha(\boldsymbol{x}, \boldsymbol{c}_\alpha, t) = \frac{1}{\pi^{(L/2)}} \int h_\alpha \exp\left(-\eta_\alpha^2\right) d\boldsymbol{\eta}_\alpha, \tag{19a}$$

$$\theta_\alpha(\boldsymbol{x}, \boldsymbol{c}_\alpha, t) = \frac{1}{\pi^{(L/2)}} \int \left(\eta_\alpha^2 - \frac{L}{2} \right) h_\alpha \exp\left(-\eta_\alpha^2\right) d\boldsymbol{\eta}_\alpha. \tag{19b}$$

The evolution equations for g_α and θ_α can be deduced from Eq. (9)

$$\frac{\partial g_\alpha}{\partial t} + \hat{\boldsymbol{c}}_\alpha \cdot \frac{\partial g_\alpha}{\partial \boldsymbol{x}} = H\sqrt{\frac{m}{2k_BT_0}}\tilde{L}_\alpha g, \tag{20a}$$

$$\frac{\partial \theta_\alpha}{\partial t} + \hat{\boldsymbol{c}}_\alpha \cdot \frac{\partial \theta_\alpha}{\partial \boldsymbol{x}} = H\sqrt{\frac{m}{2k_BT_0}}\tilde{L}_\alpha \theta, \tag{20b}$$

where $\tilde{L}_\alpha g$ and $\tilde{L}_\alpha \theta$ are the reduced collision terms defined as

$$\tilde{L}_\alpha g = \frac{1}{\pi^{(L/2)}} \int L_\alpha h \cdot \exp\left(-\eta_\alpha^2\right) d\boldsymbol{\eta}_\alpha = G_\alpha - \gamma_\alpha g_\alpha, \tag{21a}$$

$$\tilde{L}_\alpha \theta = \frac{1}{\pi^{(L/2)}} \int \left(\eta_\alpha^2 - \frac{L}{2}\right) L_\alpha h \cdot \exp\left(-\eta_\alpha^2\right) d\boldsymbol{\eta}_\alpha = \Theta_\alpha - \gamma_\alpha \theta_\alpha, \tag{21b}$$

where the complicated formulas of $\tilde{L}_\alpha g$ and $\tilde{L}_\alpha \theta$ are expressed in a simple form by introducing G_α and Θ_α, which have the following forms

$$\begin{aligned}
G_\alpha =& \gamma_\alpha n_\alpha + 2\sqrt{\frac{m_\alpha}{m}}\left[\gamma_\alpha u_{\alpha i} - \nu_{\alpha\beta}^{(1)}(u_{\alpha i} - u_{\beta i}) - \nu_{\alpha\beta}^{(2)}(q_{\alpha i} - \frac{m_\alpha}{m_\beta} q_{\beta i})\right] c_{\alpha i} \\
&+ \left[\gamma_\alpha T_\alpha - 2\frac{m_{\alpha\beta}}{m_\beta}(T_\alpha - T_\beta)\nu_{\alpha\beta}^{(1)}\right]\left(c_\alpha^2 + \frac{L}{2} - \frac{3}{2}\right) \\
&+ 2\left[(\gamma_\alpha - \nu_{\alpha\alpha}^{(3)} + \nu_{\alpha\alpha}^{(4)} + \nu_{\alpha\beta}^{(3)})P_{\alpha ik} + \nu_{\alpha\beta}^{(4)} P_{\beta ik}\right] c_{\alpha i} c_{\alpha k} \\
&+ 2\left[(\gamma_\alpha - \nu_{\alpha\alpha}^{(3)} + \nu_{\alpha\alpha}^{(4)} + \nu_{\alpha\beta}^{(3)})P_{\alpha\tau\tau} + \nu_{\alpha\beta}^{(4)} P_{\beta\tau\tau}\right] c_{\alpha\tau} c_{\alpha\tau} \\
&+ \frac{8}{5}\sqrt{\frac{m_\alpha}{m}}\left[(\gamma_\alpha - \nu_{\alpha\alpha}^{(5)} + \nu_{\alpha\alpha}^{(6)} - \nu_{\alpha\beta}^{(5)})q_{\alpha i} + \nu_{\alpha\beta}^{(6)}\sqrt{\frac{m_\beta}{m_\alpha}} q_{\beta i} - \frac{5}{8}\nu_{\alpha\beta}^{(2)}(u_{\alpha i} - u_{\beta i})\right] c_{\alpha i}\left(c_\alpha^2 + \frac{L}{2} - \frac{5}{2}\right),
\end{aligned} \tag{22}$$

and

$$\begin{aligned}
\Theta_\alpha =& -\gamma_\alpha \theta_\alpha + \left[\gamma_\alpha T_\alpha - 2\frac{m_{\alpha\beta}}{m_\beta}(T_\alpha - T_\beta)\nu_{\alpha\beta}^{(1)}\right]\left(\frac{5L}{4} - \frac{1}{2} - \frac{L^2}{4}\right) \\
&- \frac{1}{2}\left[(\gamma_\alpha - \nu_{\alpha\alpha}^{(3)} + \nu_{\alpha\alpha}^{(4)} + \nu_{\alpha\beta}^{(3)})P_{\alpha\tau\tau} + \nu_{\alpha\beta}^{(4)} P_{\beta\tau\tau}\right] \\
&+ \frac{8}{5}\sqrt{\frac{m_\alpha}{m}}\left[(\gamma_\alpha - \nu_{\alpha\alpha}^{(5)} + \nu_{\alpha\alpha}^{(6)} - \nu_{\alpha\beta}^{(5)})q_{\alpha i} + \nu_{\alpha\beta}^{(6)}\sqrt{\frac{m_\beta}{m_\alpha}} q_{\beta i} - \frac{5}{8}\nu_{\alpha\beta}^{(2)}(u_{\alpha i} - u_{\beta i})\right] c_{\alpha i}\left(\frac{5L}{4} - \frac{1}{2} - \frac{L^2}{4}\right),
\end{aligned} \tag{23}$$

for $i, k = 1, \ldots, D$ and $\tau = (D+1), \ldots, 3$.

According to Eq. (17), the macroscopic quantities can be given by the moments of the

reduced distribution functions as

$$n_\alpha = \frac{1}{\pi^{(D/2)}} \int g_\alpha \exp\left(-c_\alpha^2\right) d\boldsymbol{c}_\alpha, \tag{24a}$$

$$u_{\alpha i} = \frac{1}{\pi^{(D/2)}} \sqrt{\frac{m}{m_\alpha}} \int c_{\alpha i} g_\alpha \exp\left(-c_\alpha^2\right) d\boldsymbol{c}_\alpha, \tag{24b}$$

$$P_{\alpha ik} = \frac{1}{\pi^{(D/2)}} \int c_{\alpha i} c_{\alpha k} g_\alpha \exp\left(-c_\alpha^2\right) d\boldsymbol{c}_\alpha, \tag{24c}$$

$$P_{\alpha ii} = \frac{1}{\pi^{(D/2)}} \int \frac{1}{3} \left[\left(2c_{\alpha i}^2 - c_{\alpha k}^2 - \frac{L}{2} \right) g_\alpha - \theta_\alpha \right] \exp\left(-c_\alpha^2\right) d\boldsymbol{c}_\alpha, \tag{24d}$$

$$T_\alpha = \frac{1}{\pi^{(D/2)}} \int \left[\left(\frac{2}{3} c_\alpha^2 - 1 + \frac{L}{3} \right) g_\alpha + \frac{2}{3} \theta_\alpha \right] \exp\left(-c_\alpha^2\right) d\boldsymbol{c}_\alpha, \tag{24e}$$

$$q_{\alpha i} = \frac{1}{\pi^{(D/2)}} \sqrt{\frac{m}{m_\alpha}} \int \frac{1}{2} c_{\alpha i} \left[\left(c_\alpha^2 - \frac{5}{2} + \frac{L}{2} \right) g_\alpha + \theta_\alpha \right] \exp\left(-c_\alpha^2\right) d\boldsymbol{c}_\alpha, \tag{24f}$$

where $i, k = 1, \ldots, D$ and $i \neq k$.

III. DISCRETE UNIFIED GAS KINETIC SCHEME

A. Finite-volume discretization

The DUGKS for binary gas mixtures is constructed based on the two reduced kinetic equations (20), which can be rewritten as

$$\frac{\partial \phi_\alpha}{\partial t} + \hat{\boldsymbol{c}}_\alpha \cdot \frac{\partial \phi_\alpha}{\partial \boldsymbol{x}} = Q_\alpha = H \sqrt{\frac{m}{2k_B T_0}} \tilde{L}_\alpha \phi = \omega(\Phi_\alpha - \gamma_\alpha \phi_\alpha), \tag{25}$$

where $\phi_\alpha = g_\alpha$ or θ_α, $\Phi_\alpha = G_\alpha$ or Θ_α, and $\omega = H\sqrt{m/(2k_B T_0)}$. To solve Eq. (25), the computation domain is first divided into a set of control volumes (cells). Then integrating Eq. (25) over a control volume V_j centered at $\boldsymbol{x}_j$ from time t_n to t_{n+1}, with the midpoint rule for the time integration of the convective term and trapezoidal rule for the collision term, leads to the following scheme

$$\phi_{\alpha,j}^{n+1}(\boldsymbol{c}_\alpha) - \phi_{\alpha,j}^{n}(\boldsymbol{c}_\alpha) = -\frac{\Delta t}{|V_j|} \mathcal{F}_{\alpha,j}^{n+1/2}(\hat{\boldsymbol{c}}_\alpha) + \frac{\Delta t}{2} \left[Q_{\alpha,j}^{n}(\boldsymbol{c}_\alpha) + Q_{\alpha,j}^{n+1}(\boldsymbol{c}_\alpha) \right], \tag{26}$$

which can be rewritten as

$$\phi_{\alpha,j}^{n+1}(\boldsymbol{c}_\alpha) - \frac{\Delta t}{2} Q_{\alpha,j}^{n+1}(\boldsymbol{c}_\alpha) = \phi_{\alpha,j}^{n}(\boldsymbol{c}_\alpha) + \frac{\Delta t}{2} Q_{\alpha,j}^{n}(\boldsymbol{c}_\alpha) - \frac{\Delta t}{|V_j|} \mathcal{F}_{\alpha,j}^{n+1/2}(\hat{\boldsymbol{c}}_\alpha), \tag{27}$$

where $\Delta t = t_{n+1} - t_n$ is the time step, $|V_j|$ is the volume of the cell V_j, and the term $\mathcal{F}_{\alpha,j}^{n+1/2}$ is the flux of distribution function across the cell interface

$$\mathcal{F}_{\alpha,j}^{n+1/2}(\hat{\boldsymbol{c}}_\alpha) = \int_{\partial V_j} (\hat{\boldsymbol{c}}_\alpha \cdot \boldsymbol{n}) \phi_\alpha(\boldsymbol{x}, \boldsymbol{c}_\alpha, t_{n+1/2}) d\boldsymbol{S}, \tag{28}$$

where $\boldsymbol{n}$ is the outward unit vector normal to the cell surface ∂V_j and $\phi^n_{\alpha,j}$ and $Q^n_{\alpha,j}$ in Eq. (26) are the cell averaged values of ϕ_α and Q_α defined by

$$\phi^n_{\alpha,j}(\boldsymbol{c}_\alpha) = \frac{1}{|V_j|}\int_{V_j} \phi_\alpha(\boldsymbol{x}, \boldsymbol{c}_\alpha, t_n) d\boldsymbol{x}, \tag{29a}$$

$$Q^n_{\alpha,j}(\boldsymbol{c}_\alpha) = \frac{1}{|V_j|}\int_{V_j} Q_\alpha(\boldsymbol{x}, \boldsymbol{c}_\alpha, t_n) d\boldsymbol{x}. \tag{29b}$$

The updating rule given by Eq. (26) is implicit due to the term $Q^{n+1}_{\alpha,j}$. In order to remove the implicitness of the collision term and obtain an explicit form as in the original DUGKS for single gas flows, we introduce two new distribution functions

$$\tilde{\phi}_\alpha = \phi_\alpha - \frac{\Delta t}{2} Q_\alpha = \left(1 + \frac{\Delta t}{2}\omega_\alpha \gamma_\alpha\right)\phi_\alpha - \frac{\Delta t}{2}\omega_\alpha \Phi_\alpha, \tag{30a}$$

$$\tilde{\phi}^+_\alpha = \phi_\alpha + \frac{\Delta t}{2} Q_\alpha = \left(1 - \frac{\Delta t}{2}\omega_\alpha \gamma_\alpha\right)\phi_\alpha + \frac{\Delta t}{2}\omega_\alpha \Phi_\alpha. \tag{30b}$$

Then Eq. (26) can be rewritten as

$$\tilde{\phi}^{n+1}_{\alpha,j} = \tilde{\phi}^{+,n}_{\alpha,j} - \frac{\Delta t}{|V_j|}\mathcal{F}^{n+1/2}_{\alpha,j}(\hat{\boldsymbol{c}}_\alpha). \tag{31}$$

In the simulations, we can track the evolution of $\tilde{\phi}_\alpha$ instead of the original distribution function ϕ_α to avoid the implicity of Eq. (26).

The macroscopic quantities can be calculated from the moments of $\tilde{g}_\alpha$ and $\tilde{\theta}_\alpha$ according to Eqs. (24) and (30). The moments of Φ_α are also involved, which have complicated formations due to the complex expressions of Φ_α. Details for solving the equation system for the macroscopic quantities can be found in Appendix A. According to the linearized expression of the collision term, the equation system for the macroscopic quantities can be solved explicitly.

B. Flux evaluation

The key in DUGKS is to evaluate the flux $\mathcal{F}^{n+1/2}$ when updating $\tilde{\phi}^{n+1}_{\alpha,j}$ as shown in Eq. (31). According to Eq. (28), $\mathcal{F}^{n+1/2}(\hat{\boldsymbol{c}}_\alpha)$ is determined by the distribution function $\phi_\alpha(\boldsymbol{x}, \boldsymbol{c}_\alpha, t_{n+1/2})$ at the cell interface. To this end, we integrate Eq. (25) along the characteristic line from time t_n to $t_{n+1/2}$,

$$\phi_\alpha(\boldsymbol{x}_b, \boldsymbol{c}_\alpha, t_n + s) - \phi_\alpha\left(\boldsymbol{x}_b - \hat{\boldsymbol{c}}_\alpha s, \boldsymbol{c}_\alpha, t_n\right) = \frac{s}{2}\left[Q_\alpha(\boldsymbol{x}_b, \boldsymbol{c}_\alpha, t_n + s) + Q_\alpha\left(\boldsymbol{x}_b - \hat{\boldsymbol{c}}_\alpha s, \boldsymbol{c}_\alpha, t_n\right)\right], \tag{32}$$

where $s = \Delta t/2$, $\boldsymbol{x}_b$ is the interface center of cell j, and the trapezoidal rule is employed again to evaluate the collision term. The implicity caused by the term $Q_\alpha^{n+1/2}$ can be removed by introducing another two auxiliary distribution functions,

$$\bar{\phi}_\alpha = \phi_\alpha - \frac{\Delta s}{2} Q_\alpha = \left(1 + \frac{\Delta s}{2}\omega\gamma_\alpha\right)\phi_\alpha - \frac{\Delta s}{2}\omega\Phi_\alpha, \tag{33a}$$

$$\bar{\phi}_\alpha^+ = \phi_\alpha + \frac{\Delta s}{2} Q_\alpha = \left(1 - \frac{\Delta s}{2}\omega\gamma_\alpha\right)\phi_\alpha + \frac{\Delta s}{2}\omega\Phi_\alpha. \tag{33b}$$

Then Eq. (32) can then be rewritten as

$$\bar{\phi}_\alpha(\boldsymbol{x}_b, \boldsymbol{c}_\alpha, t_{n+1/2}) = \bar{\phi}_\alpha^+\left(\boldsymbol{x}_b - \hat{\boldsymbol{c}}_\alpha s, \boldsymbol{c}_\alpha, t_n\right), \tag{34}$$

where

$$\bar{\phi}_\alpha^+\left(\boldsymbol{x}_b - \hat{\boldsymbol{c}}_\alpha s, \boldsymbol{c}_\alpha, t_n\right) = \bar{\phi}_\alpha^+(\boldsymbol{x}_j, \boldsymbol{c}_\alpha, t_n) + (\boldsymbol{x}_b - \boldsymbol{x}_j - \hat{\boldsymbol{c}}_\alpha s)\cdot\boldsymbol{\delta}_j, \tag{35}$$

where $(\boldsymbol{x}_b - \hat{\boldsymbol{c}}_\alpha s) \in V_j$ and $\boldsymbol{\delta}_j$ is the slope of $\bar{\phi}_\alpha^+$ in cell j. We take the one-dimensional case for example. The distribution function ϕ_α at the cell interface $x_b = x_{j+1/2}$ can be reconstructed by approximating the distribution function $\bar{\phi}_\alpha^+$ as

$$\bar{\phi}_\alpha^+\left(x_b - \hat{c}_\alpha s, c_\alpha, t_n\right) = \begin{cases} \bar{\phi}_\alpha^+(x_j, c_\alpha, t_n) + (x_b - x_j - \hat{c}_\alpha s)\cdot\delta_j, & \hat{c}_\alpha > 0, \\ \bar{\phi}_\alpha^+(x_{j+1}, c_\alpha, t_n) + (x_b - x_{j+1} - \hat{c}_\alpha s)\cdot\delta_j, & \hat{c}_\alpha < 0. \end{cases} \tag{36}$$

The slope $\boldsymbol{\delta}_j$ can be approximated by the the van Leer limiter[53] for discontinuous problems. Once the distribution function $\bar{\phi}_\alpha$ at the interface is known, the original distribution function ϕ_α can be obtained according to Eq. (33),

$$\phi_\alpha(\boldsymbol{x}_b, \boldsymbol{c}_\alpha, t_{n+1/2}) = \frac{2}{2 + s\omega\gamma_\alpha}\bar{\phi}_\alpha(\boldsymbol{x}_b, \boldsymbol{c}_\alpha, t_{n+1/2}) + \frac{s\omega}{2 + s\omega\gamma_\alpha}\Phi_\alpha(\boldsymbol{x}_b, \boldsymbol{c}_\alpha, t_{n+1/2}). \tag{37}$$

Note that the macroscopic quantities used to evaluate the distribution function Φ_α can be obtained from $\bar{\phi}_\alpha$, which is similar to the previous treatment of cell averaged macroscopic variables presented in Appendix A.

In numerical simulations, the velocity space is discretized into a set of discrete velocities $\boldsymbol{c}_{\alpha k}(k = 1, 2, \ldots, b)$. Usually, the proper quadrature rules are chosen to discretize the velocity space and approximate the moments. For example, the number density n_α of species α can be obtained as

$$n_\alpha = \frac{1}{\pi^{(D/2)}}\sum_k w_k \tilde{g}_\alpha(\boldsymbol{c}_{\alpha k})\exp\left(-c_{\alpha k}^2\right), \tag{38}$$

where w_k are the quadrature weights.

It is noted that the time step in DUGKS is determined only by the Courant-Friedrichs-Lewy(CFL) condition, i.e.,

$$\Delta t = \eta \frac{x_{min}}{\max\left(|\hat{\boldsymbol{c}}_A|, |\hat{\boldsymbol{c}}_B|\right)}, \tag{39}$$

where $0 < \eta < 1$ is the CFL number and x_{min} is the minimal mesh size. The particle transport and collision effects are coupled in determining the numerical flux across a cell interface, so that the time step Δt of the DUGKS is not limited by the particle collision time but determined by the CFL number. Due to its nice asymptotic preserving (AP) property[38,54], the DUGKS can change self-dynamically from the hydrodynamic to the free-molecular flow regimes. It is also noted that the midpoint and trapezoidal rules used in Eqs. (26) and (32), as well as the linear reconstruction of the distribution function at the cell interface, ensure a second-order accuracy in both temporal and spatial discretizations. It has been demonstrated that the DUGKS has a second-order accuracy in space[55,56].

C. Algorithm

In summary, the calculation procedure of the DUGKS for binary gas mixtures described by the McCormack model from t_n to t_{n+1} can be listed as follows:

1. Compute $\tilde{\phi}_\alpha^{+,n}$ and $\bar{\phi}_\alpha^{+,n}$ in each cell according to Eqs. (30) and (33), respectively.

2. Reconstruct the distribution function $\bar{\phi}_\alpha^{+}(\boldsymbol{x}_b - \hat{\boldsymbol{c}}_\alpha s, \boldsymbol{\xi}, t_n)$ according to Eq. (35).

3. Determine the distribution function $\bar{\phi}_\alpha(\boldsymbol{x}_b, \boldsymbol{c}_\alpha, t_{n+1/2})$ according to Eq. (34).

4. Compute the quantities appeared in the collision term at cell interface $\boldsymbol{x}_b$ at time $t_{n+1/2}$ according to Eqs. (24) and (33).

5. Compute the original distribution function at each cell interface $\boldsymbol{x}_b$ at time $t_{n+1/2}$, i.e., $\phi_\alpha(\boldsymbol{x}_b, \boldsymbol{c}_\alpha, t_{n+1/2})$, according to Eq. (37).

6. Compute the flux $\mathcal{F}^{n+1/2}$ through each cell interface from $\phi_\alpha(\boldsymbol{x}_b, \boldsymbol{c}_\alpha, t_{n+1/2})$ according to Eq. (28).

7. Update the cell-averaged distribution function $\tilde{\phi}_\alpha$ in each cell according to Eq. (31).

IV. NUMERICAL EXAMPLES

In this section, the proposed DUGKS will be applied to several problems, including the Couette flow, the lid-driven cavity flow, and the Fourier flow over a wide range of Knudsen number. In each test, different mass ratios and molar concentrations will be considered.

For the the Couette and lid-driven cavity flow, the flow field is assumed to be steady when the maximum relative change of the velocity field of the two species in two successive steps is less than 10^{-10}, i.e.,

$$\max\left(\frac{|u_A^{n+1}-u_{A,}^n|}{|u_A^n|},\frac{|u_B^{n+1}-u_B^n|}{|u_B^n|}\right)<10^{-10}, \tag{40}$$

where the maximum is taken over the whole domain. For the Fourier flow, the flow field is steady when the maximum relative change of the quantity q_A and q_B in two-successive steps is less than 10^{-10}.

Two groups of binary gas mixtures of noble gases with different mass ratios are considered, i.e., neon-argon (Ne-Ar) and helium-xenon (He-Xe). The molecular masses of these gases are $m_{He}=4.0026$, $m_{Ne}=20.1791$, $m_{Ar}=39.948$, and $m_{Xe}=131.293$ in atomic units. The hard sphere model is chosen as the intermolecular potential. For Ne-Ar and He-Xe mixtures, the molecular diameter ratios are $d_B/d_A=1.406$ and 2.226 at an equilibrium temperature $T_0=300K$. All flows are characterized by the following rarefaction parameter[57]

$$\delta=\frac{Hp_0}{\mu v_0}, \tag{41}$$

where μ is the mixture viscosity at temperature T_0 according to Eq. (16). Since the Knudsen number is defined as $\mathrm{Kn}=\lambda/H$, where λ is the mean free path of the mixture and can be given as[29]

$$\lambda=\frac{\mu}{p_0}\sqrt{\frac{\pi k_B T_0}{2m}}. \tag{42}$$

Then rarefaction parameter δ and the Knudsen number Kn have the following relationship: $\delta=\sqrt{\pi}/(2\mathrm{Kn})$.

A. Couette flow

Now we apply the DUGKS to the plane Couette flow of binary gas mixtures for different rarefaction degrees. As shown in Fig. 1, two parallel plates with a constant temperature

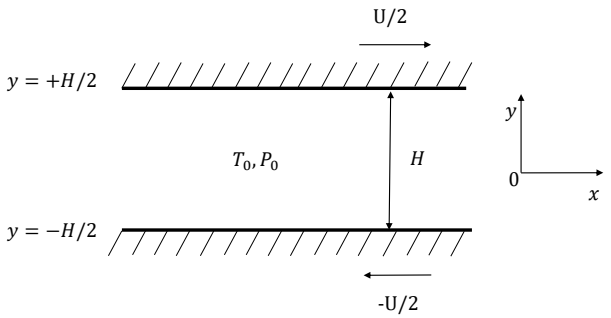

FIG. 1: Schematic of the plane Couette flow.

T_0 are located at $y = \pm H/2$, respectively. The top and bottom walls move with velocities $\pm U/2$ in the x direction, respectively. Here we assume that the plate velocities are much smaller than the characteristic molecular velocity v_0 of mixture, i.e.,

$$\epsilon = \frac{U}{v_0} \ll 1. \tag{43}$$

The periodic boundary conditions are imposed on the inlet and outlet of the channel. The Maxwell diffuse-specular boundary condition is applied to describe the gas-wall interaction. For the linearized Couette flow, the boundary conditions have the following forms

$$g_\alpha^{(out)}(y = \pm H/2) = (1 - a_\alpha) g_\alpha^{(in)}(y = \pm H/2) \pm a_\alpha \sqrt{\frac{m_\alpha}{m}} c_{\alpha x}, \tag{44a}$$

$$\theta_\alpha^{(out)}(y = \pm H/2) = 0, \tag{44b}$$

where a_α is the accommodation coefficient of the species α, the superscripts 'out' refers to the molecules leaving the plates' surface after hitting the walls and 'in' refers to the molecules moving to the walls. In this paper, we assume the plates are fully diffusive (i.e., $a_\alpha = 1$) for all cases. In this case, we focus on the shear stress P_{xy} of the mixture according to Eq. (18) and the velocity $u_{\alpha x}$ of species α according to Eq. (24).

Several values of δ are considered, i.e., $\delta = 0.1, 1, 10, 100$, and 1000 (Kn = 8.86, 0.886, 0.0886, 0.00886, and 0.00089 correspondingly). The half-range Gauss-Hermite quadrature[58] is adopted for each species with 8×8 velocity points for $\delta = 1000$ and 28×28 for $\delta = 100, 10, 1$. The trapezoidal rule[59,60] is used to discretize velocity space ($c_{\alpha x}, c_{\alpha y} \in [-4, 4]$) with 32×32 nonuniform grid points for $\delta = 0.1$ for each species. The physical space is divided nonuniformly into $N_x = 2$ grid points in the x direction and $N_y = 21$ in the y direction, in which the location of the volume center (x_i, y_j) is generated by the following

formulations,

$$x_i = \frac{(\zeta_i + \zeta_{i+1})}{2}, \quad y_j = \frac{(\zeta_j + \zeta_{j+1})}{2} \tag{45}$$

where

$$\zeta_i = \frac{1}{2} + \frac{\tanh\left[a(i/N_{x,y} - 0.5)\right]}{2\tanh(a/2)}, \quad i = 0, 1, ..., N_{x,y} - 1, \tag{46}$$

with a being the constant used to determine the distribution of the mesh. The mesh near the walls can be refined by increasing a. Here we set $a = 1$ in the x direction and 3.5 in the y direction. The CFL number is set to be 0.4 in the following cases.

The results of $\delta = 0.1$, 1, and 10 from the present DUGKS will be compared with the DVM solutions of the McCormack model[22,27], where the spatial derivative is approximated by the second-order upwind finite-difference method and the physical space is discretized by 100 points nonuniformly. It is noted that the mesh size in DUGKS is not needed to be smaller than the mean free path of molecules, thus coarser meshes can be employed in the DUGKS than those in the traditional DVM for flows in continuum and near-continuum regimes[61,62]. Comparisons have been made between the DUGKS and the traditional third-order time-implicit Godunov DVM (GDVM) by Wang et al.[63]. Results show that the DUGKS requires less spatial resolution than that of the GDVM to achieve the same numerical accuracy in the near-continuum regimes. Besides, mesh independence in the spatial and molecular velocity spaces have been carefully evaluated. It is noted that the GDVM does not give a converged result in the continuum regime due to the large dissipation. In this test, the cases of $\delta = 100$ and 1000 are also simulated and the cell size of DUGKS for $\delta = 1000$ are about 13 to 99 times of the mean free path. Actually, as $\delta = 1000$, the flow is continuous and can be described by the Navier-Stokes equations. Analytical solutions of velocity and shear stress in hydrodynamic regime have been given as[22]

$$u_x = y, \quad P_{xy} = \frac{1}{2\delta}, \tag{47}$$

which will also be included in this paper to compare with the DUGKS results.

The velocity profiles for the Ne-Ar mixture with molar concentration $C_0 = 0.5$ are demonstrated in Fig. 2. It is clear that the results predicted by the DUGKS agree well with those by the DVM at $\delta = 0.1$, 1, and 10 for the small mass ratio case. To illustrate the influence of the mass ratio, the velocity of the He-Xe mixture is also shown in Fig. 3. It can be seen that the nonlinearity of the velocity profiles near the wall is successfully captured by both

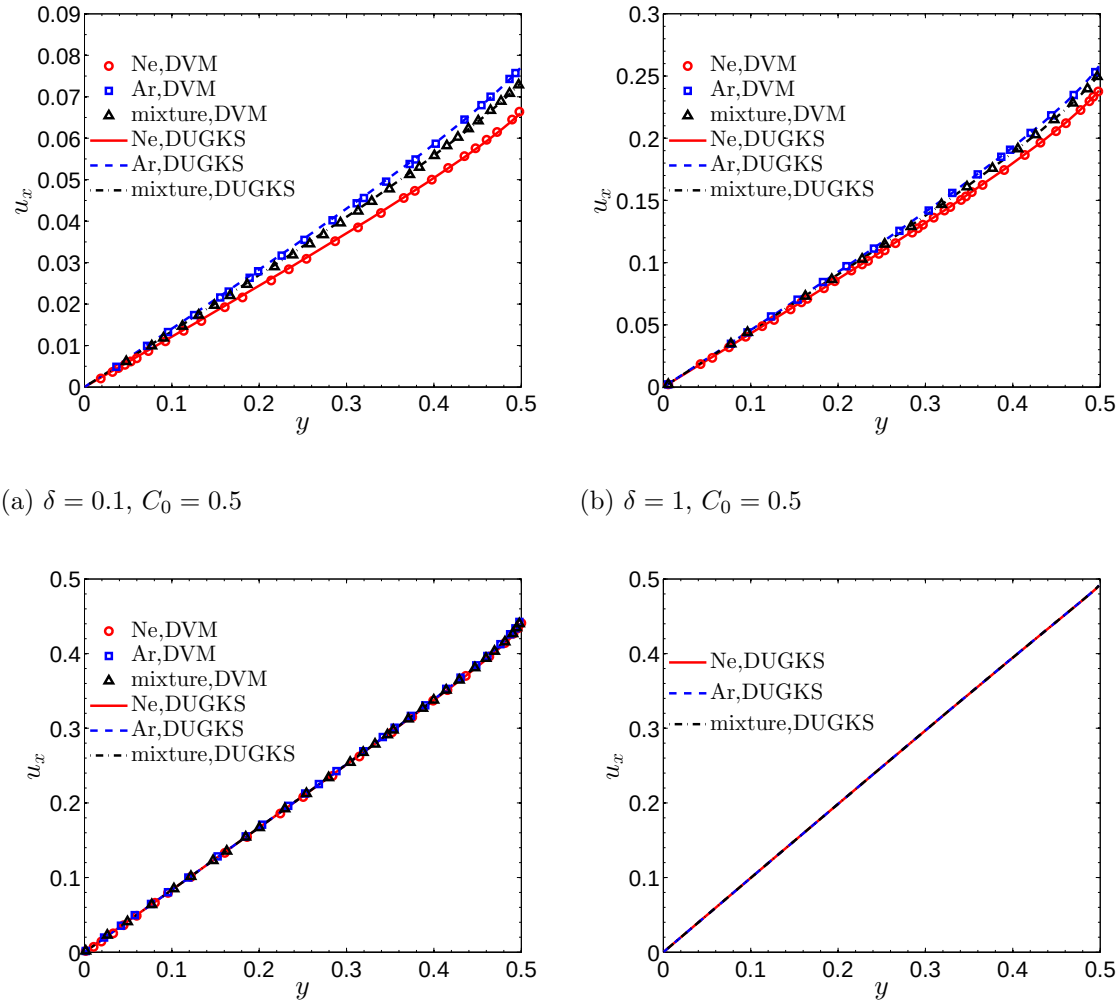

(a) $\delta = 0.1$, $C_0 = 0.5$

(b) $\delta = 1$, $C_0 = 0.5$

(c) $\delta = 10$, $C_0 = 0.5$

(d) $\delta = 100$, $C_0 = 0.5$

FIG. 2: Velocity profiles of the Couette flow for the Ne-Ar mixture with $C_0 = 0.5$.

the DUGKS and the DVM under large mass ratio. We also present the results of DUGKS for $\delta = 100$ under both small and large mass ratios in Figs. 2(d) and 3(d). The results of $\delta = 1000$ are similar to those of $\delta = 100$ and are not presented here. It can be seen that differences between velocity of each species become very small due to sufficient intermolecular collisions with increasing δ.

The influence of the molar concentration C_0 on the gas velocity at the plate is displayed in Table I with $\delta = 0.1, 1, 10, 100$, and 1000. As can be seen, the relative differences in the Ne and Ar velocities between the DUGKS and the DVM are both less than 0.1% for all values of C_0 as $\delta = 0.1, 1$, and 10. As $\delta = 100$ and 1000, the DUGKS results show that

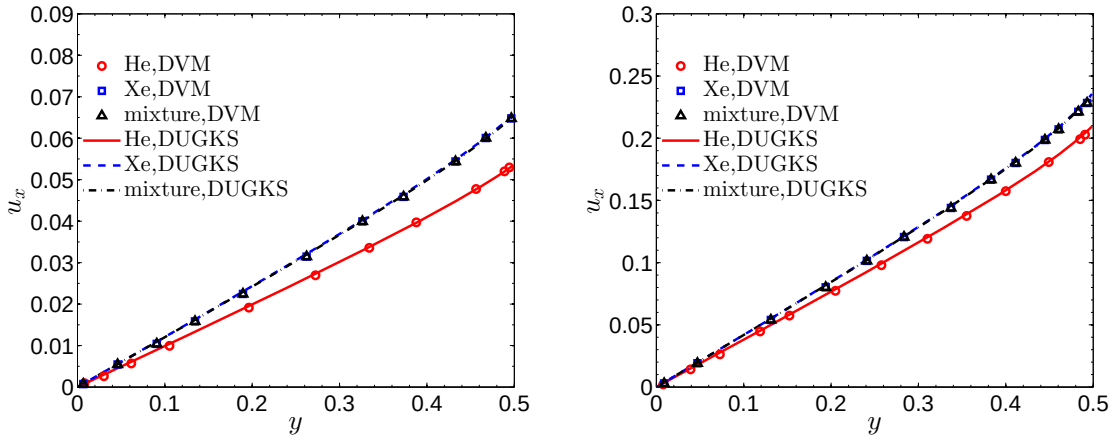

(a) $\delta = 0.1$, $C_0 = 0.5$ (b) $\delta = 1$, $C_0 = 0.5$

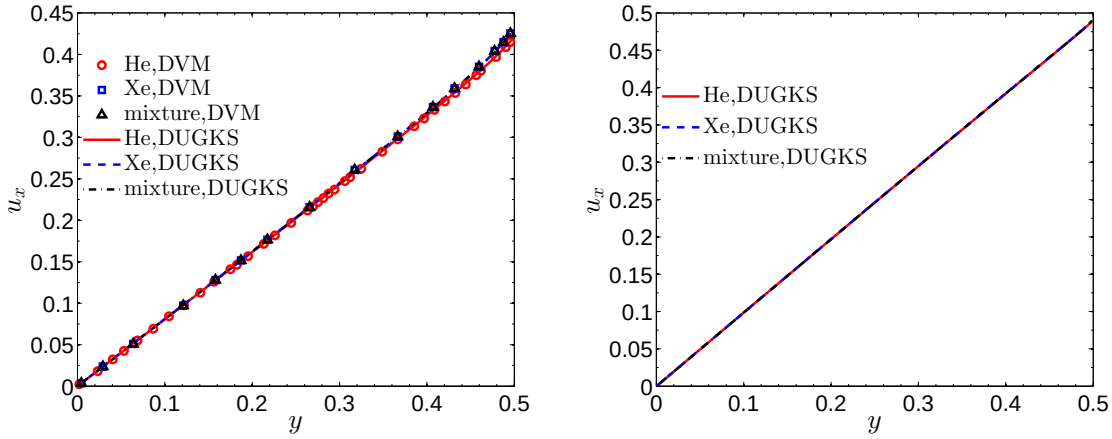

(c) $\delta = 10$, $C_0 = 0.5$ (d) $\delta = 100$, $C_0 = 0.5$

FIG. 3: Velocity profiles of the Couette flow for the He-Xe mixture with $C_0 = 0.5$.

the molar concentration C_0 almost has no clear influence on the velocities of Ne and Ar. At sufficiently high δ, the species velocities become indistinguishable. In addition, with a fixed δ, the mixture velocity doesn't change with C_0. Furthermore, good agreement can be found between the DUGKS results and the analytical solution listed in the 3rd, 5th, and 7th columns of Table I as $\delta = 1000$ and C_0 varies from 0.1 to 0.9, which confirms that the DUGKS can capture the continuous flow behaviors.

The shear stresses P_{xy} of the Ne-Ar and He-Xe mixtures are summarized in Table II under different values of δ and C_0. From the theoretical prospect, the shear stress of each mixture should be constant due to the momentum conservation of the mixture. While slight

TABLE I: Species velocity u_{Ne} and u_{Ar} and mixture velocity u_m at $y = H/2$ for the Ne-Ar mixture with concentration of the light species C_0 and rarefaction parameter δ.

δ	u_{Ne}		u_{Ar}		u_m	
	Present	Ho et al.[27]	Present	Ho et al.[27]	Present	Ho et al.[27]
			$C_0 = 0.1$			
0.1	0.0634	0.0633	0.0736	0.0736	0.0731	0.0730
1	0.2340	0.2341	0.2535	0.2536	0.2525	0.2525
10	0.4358	0.4361	0.4417	0.4420	0.4414	0.4417
100	0.4923	—	0.4930	—	0.4930	—
1000	0.4989	0.5	0.4989	0.5	0.4989	0.5
			$C_0 = 0.5$			
0.1	0.0663	0.0663	0.0773	0.0773	0.0736	0.0736
1	0.2399	0.2399	0.2598	0.2598	0.2531	0.2531
10	0.4374	0.4377	0.4432	0.4435	0.4413	0.4416
100	0.4928	—	0.4935	—	0.4932	—
1000	0.4991	0.5	0.4992	0.5	0.4992	0.5
			$C_0 = 0.9$			
0.1	0.0712	0.0712	0.0834	0.0833	0.0734	0.0734
1	0.2492	0.2492	0.2694	0.2695	0.2528	0.2529
10	0.4404	0.4407	0.4459	0.4463	0.4413	0.4417
100	0.4928	—	0.4935	—	0.4929	—
1000	0.4989	0.5	0.4990	0.5	0.4989	0.5

deviations from theoretical values are likely to appear in the numerical results. Therefore the average shear stress $P_{xy}^{av} = \int_{-H/2}^{H/2} P_{xy}(y)dy$ is needed here. The maximum variation of the shear stress between the plates is calculated as

$$\Delta P_{xy} = \max_{-H/2 \le y \le H/2} \left\| \frac{P_{xy}(y) - P_{xy}^{av}}{P_{xy}^{av}} \right\|, \tag{48}$$

which is less than 0.2%, indicating a good numerical accuracy of the proposed DUGKS. It is clear that the results obtained from the DUGKS agree great well with those from the reference data[22] for both the Ne-Ar and He-Xe mixtures at $\delta = 0.1, 1$, and 10. The relative

TABLE II: The shear stress P_{xy} in the Couette flow of the Ne-Ar and He-Xe mixtures under different rarefaction parameter δ and concentration of the light species C_0.

δ	$C_0 = 0.1$		$C_0 = 0.5$		$C_0 = 0.9$	
	Present	Sharipov et al.[22]	Present	Sharipov et al.[22]	Present	Sharipov et al.[22]
			Ne-Ar			
0.1	0.2601	0.2601	0.2575	0.2576	0.2594	0.2594
1	0.1688	0.1689	0.1674	0.1675	0.1685	0.1685
10	0.0415	0.0415	0.04138	0.04139	0.04146	0.04147
100	0.0049	—	0.00481	—	0.0049	—
1000	0.000498	0.0005	0.000498	0.0005	0.000498	0.0005
			He-Xe			
0.1	0.2527	0.2527	0.2163	0.2163	0.1919	0.1919
1	0.1655	0.1655	0.1482	0.1482	0.1360	0.1360
10	0.04127	0.04128	0.03998	0.03999	0.03898	0.03898
100	0.0049	—	0.00482	—	0.00486	—
1000	0.000499	0.0005	0.000498	0.0005	0.000498	0.0005

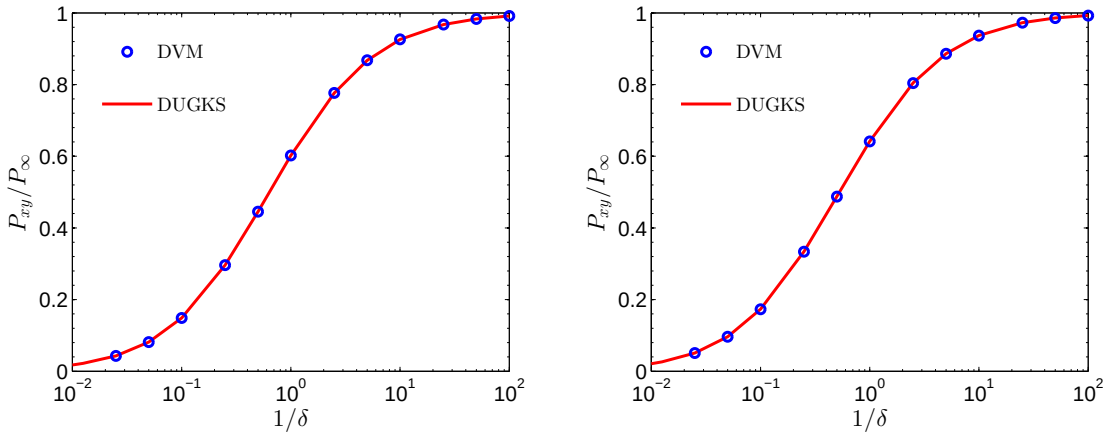

(a) Ne-Ar, $C_0 = 0.5$ (b) He-Xe, $C_0 = 0.5$

FIG. 4: The normalized stress of the Couette flow for gas mixtures under different rarefaction parameter δ with $C_0 = 0.5$.

differences in shear stress are less than 0.2% for all considered values of molar concentration C_0 as $\delta = 0.1, 1$, and 10, meaning a good agreement between the DUGKS and DVM based on the McCormack model at both small and large mass ratios. Furthermore, the DUGKS results show that the relative differences in shear stress of the Ne-Ar and He-Xe mixtures are very small under all considered C_0 at $\delta = 100$ and 1000. The analytical solution of shear stress [see Eq. (47)] is also listed in the 3rd, 5th, and 7th columns of Table II as $\delta = 1000$ for both the Ne-Ar and He-Xe mixtures. Comparisons with the analytical solutions show that the DUGKS is accurate in the continuum regime.

The influence of the rarefaction parameter δ on the shear stress is presented in Fig. 4 with $C_0 = 0.5$ for the Ne-Ar and He-Xe mixtures. As δ varies from 0.01 to 100, excellent agreement is observed between the DUGKS and the DVM results based on the McCormack model for both the Ne-Ar and the He-Xe mixtures.

TABLE III: The shear stress P_{xy} in the Couette flow of the He-Ar mixture under different rarefaction parameter δ and concentration of the light species C_0.

δ	$C_0 = 0.25$			$C_0 = 0.5$			$C_0 = 0.75$		
	AAP	DSMC	Present	AAP	DSMC	Present	AAP	DSMC	Present
0.1	0.2458	0.2442	0.2469	0.2305	0.2310	0.2335	0.2207	0.2233	0.2254
1	0.1599	0.1616	0.1628	0.1490	0.1555	0.1565	0.1425	0.1519	0.1528
10	0.04054	0.04108	0.04108	0.03931	0.04073	0.04064	0.03892	0.04044	0.04036
20	0.02239	0.02255	0.02255	0.02199	0.02244	0.2242	0.02188	0.02231	0.02233
40	0.01182	0.01185	0.01185	0.01170	0.01184	0.01182	0.01167	0.01182	0.01179

To further investigate the differences between various kinetic models for mixtures, numerical comparisons are performed among the AAP model, the linearized Boltzmann equation (LBE), the McCormack model and the full Boltzmann equation. The Couette flows for binary gas mixtures are used as comparison cases. The results of the AAP model are obtained from our previous work[46] and are shown again to make comparison with those of the other models. The LBE is solved by the DVM[27], and the Boltzmann equation is by the DSMC method[4].

Figure 5 shows the velocity profiles obtained from the AAP model, the LBE and the McCormack model for the Ne-Ar and He-Xe mixtures. As $\delta = 0.1$, the velocity profile of Ne

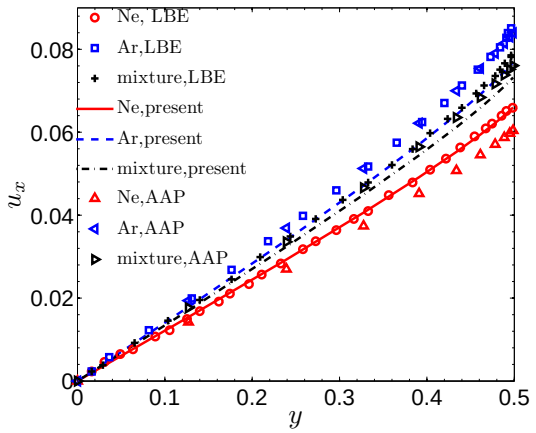

(a) Ne-Ar, $\delta = 0.1$, $C_0 = 0.5$

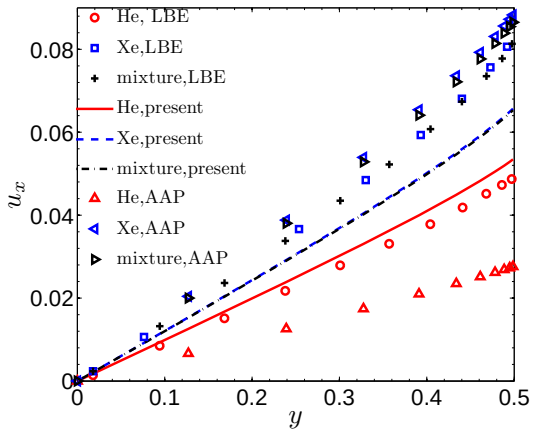

(b) He-Xe, $\delta = 0.1$, $C_0 = 0.5$

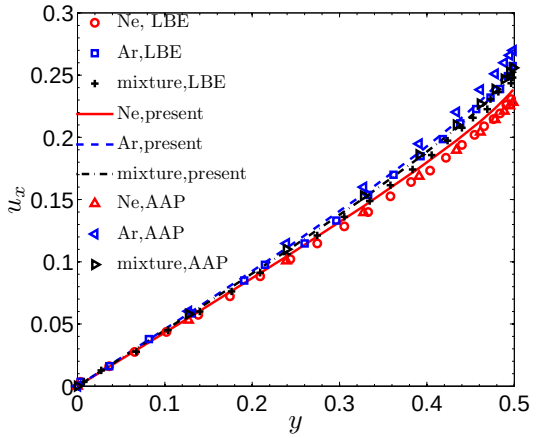

(c) Ne-Ar, $\delta = 1$, $C_0 = 0.5$

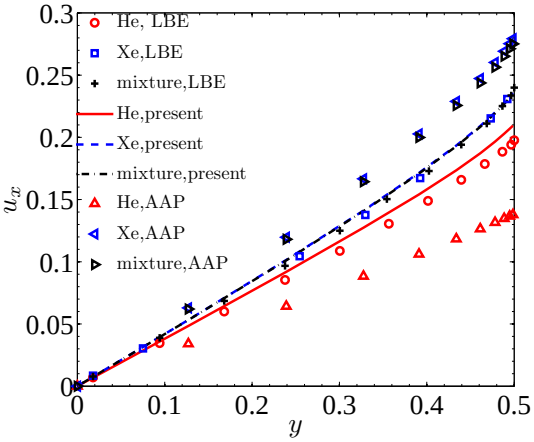

(d) He-Xe, $\delta = 1$, $C_0 = 0.5$

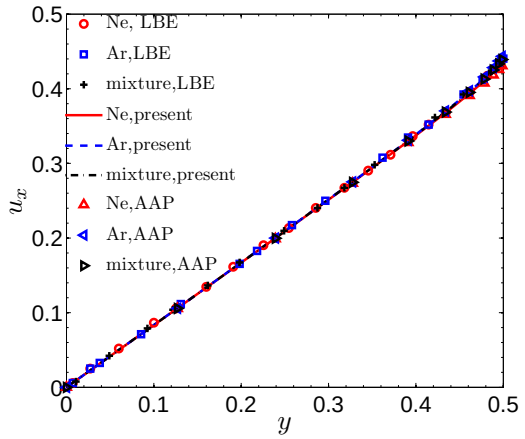

(e) Ne-Ar, $\delta = 10$, $C_0 = 0.5$

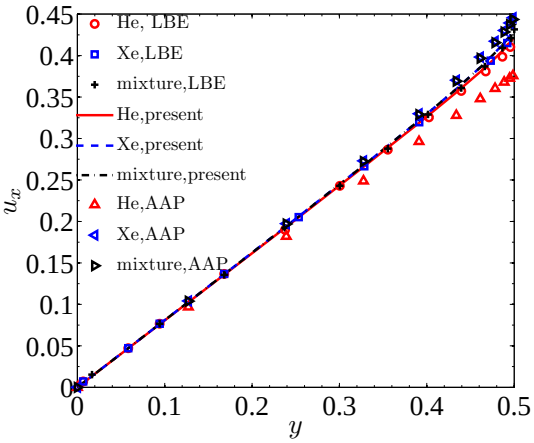

(f) He-Xe, $\delta = 10$, $C_0 = 0.5$

FIG. 5: Velocity profiles of the Couette flow for the Ne-Ar and He-Xe mixtures with $C_0 = 0.5$.

from the McCormack model agrees well that of the LBE, while the relative difference of the Ar velocity between the two models is about 9%. On the contrary, the relative difference of the Ne velocity between the LBE and the AAP model is 9%, while the velocity profile of Ar between these two models have a good agreement. Similar pattern can be found for the He-Xe mixture at $\delta = 0.1$. It can be seen that the larger the mass ratio, the larger the differences among these models in the near free-molecular regime. As $\delta = 1$, the difference in Ne velocity increases slightly between the LBE and the McCormack model, while that for the Ar velocity decreases obviously. On the contrary, the velocity profiles of the Ne between the LBE and the AAP model have a better agreement, while the relative difference of the Ar velocity between these two models increases. As for the He-Xe mixture at $\delta = 1$, good agreement can be found between the LBE and the McCormack models. However, the results of the AAP and the LBE models differ significantly in this case. When $\delta = 10$, all these models agree well for the Ne-Ar mixture, while obvious difference can be found between the LBE and the AAP model for the He-Xe mixture in this case, where the LBE and the McCormack model show good agreement.

The shear stresses P_{xy} obtained from the AAP model, the McCormack model and the DSMC method[4] is displayed in Table III for the He-Ar mixture whose mass ratio is 9.98. The rarefaction parameter δ ranges from 0.1 to 40 and $C_0 = 0.25$, 0.5 and 0.75. Good agreement between the McCormack model and the DSMC can be observed and the maximum relative difference is less than 1%, except for $\delta = 0.1$ where the relative difference is about 1%. As for the AAP model, the relative difference with the DSMC method experiences an increase first and then decrease as δ varies from 0.1 to 40. The maximum relative difference between the AAP model and the DSMC method exceeds 6% at $\delta = 1$ when $C_0 = 0.25$ and 0.75.

The above comparisons show that the McCormack model approximates solutions of the LBE and the original Boltzmann equation better than the AAP model for the large mass ratio case in the transition and near-continuum flow regimes.

B. Fourier flow

The second case is the Fourier flow of binary gas mixtures. The flow domain is confined by two parallel plates placed at $y = \pm H/2$ as shown in Fig. 6. Both plates are stationary and have the temperature $T_c = T_0 - \Delta T/2$ at $y = -H/2$ and $T_h = T_0 + \Delta T/2$ at $y = H/2$,

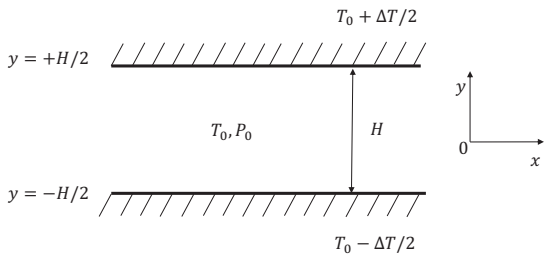

FIG. 6: Schematic of the plane Fourier flow.

where the temperature difference ΔT is much smaller than the equilibrium temperature T_0, i.e., $\epsilon = \Delta T/T_0 \ll 1$. The plates are fully diffusive and the periodic boundary conditions are imposed on the inlet and outlet of the channel. The Maxwell diffuse-specular boundary condition is applied to describe the gas-wall interaction. For the linearized Fourier flow, the boundary conditions have the following forms

$$n_\alpha(y = \pm H/2) = \pm\frac{2}{\sqrt{\pi}}\int g_\alpha^{(in)}(y = \pm H/2)\exp(-c_{\alpha x}^2 - c_{\alpha y}^2)c_{\alpha y}dc_{\alpha x}dc_{\alpha y}, \tag{49a}$$

$$g_\alpha^{(out)}(y = \pm H/2) = (1 - a_\alpha)g_\alpha^{(in)}(y = \pm H/2) + a_\alpha\left\{n_\alpha(y = \pm H/2) \pm [(c_{\alpha x}^2 + c_{\alpha y}^2)/2 - 0.75]\right\}, \tag{49b}$$

$$\theta_\alpha^{(out)}(y = \pm H/2) = (1 - a_\alpha)\theta_\alpha^{(in)}(y = \pm H/2) \pm 0.25a_\alpha. \tag{49c}$$

In this case, the deviated n_α, concentration C, deviated temperature T_α and heat flux $q_{\alpha y}$ are the interests, where the concentration C is defined as

$$C(y) = \frac{C' - C_0}{C_0\epsilon} = (1 - C_0)\left[n_A(y) - n_B(y)\right], \tag{50}$$

with

$$C' = \frac{n_{0A} + n'_A}{n_{0A} + n_{0B} + n'_A + n'_B}. \tag{51}$$

The physical space is divided nonuniformly into 2 grid points in the x direction and 21 in the y direction and the constant a in Eq. (46) have the same values with those of the Couette flow. Consequently, the mesh size for this problem is also larger than the molecular mean free path as $\delta = 1000$. The velocity space is discretized by the same rule with the same number of velocity points with those of the Couette flow. The CFL number is 0.4 in this case.

The number density profiles for the Ne-Ar and He-Xe mixtures with $C_0 = 0.5$ at $\delta = 0.1$, 1, 10, and 100 (Kn = 8.86, 0.886, 0.0886, and 0.00886 correspondingly) are shown in Figs. 7

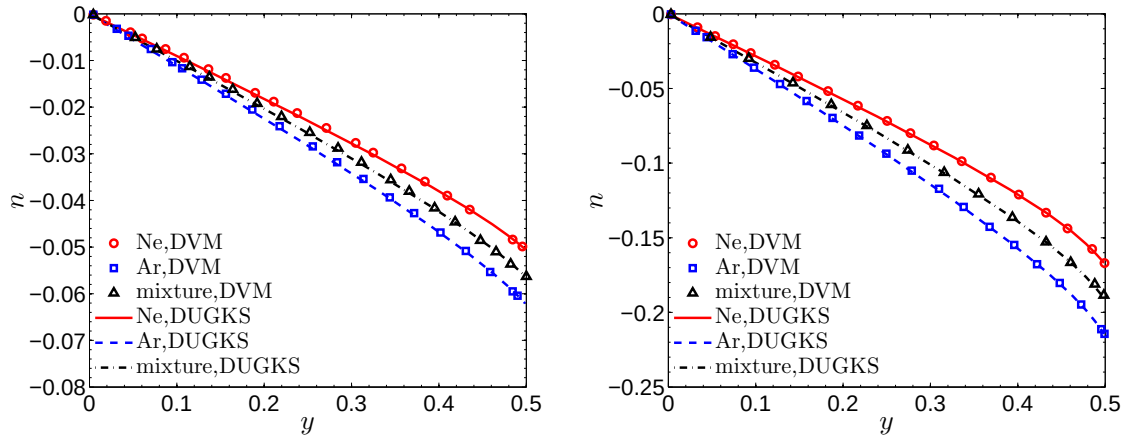

(a) $\delta = 0.1$, $C_0 = 0.5$ (b) $\delta = 1$, $C_0 = 0.5$

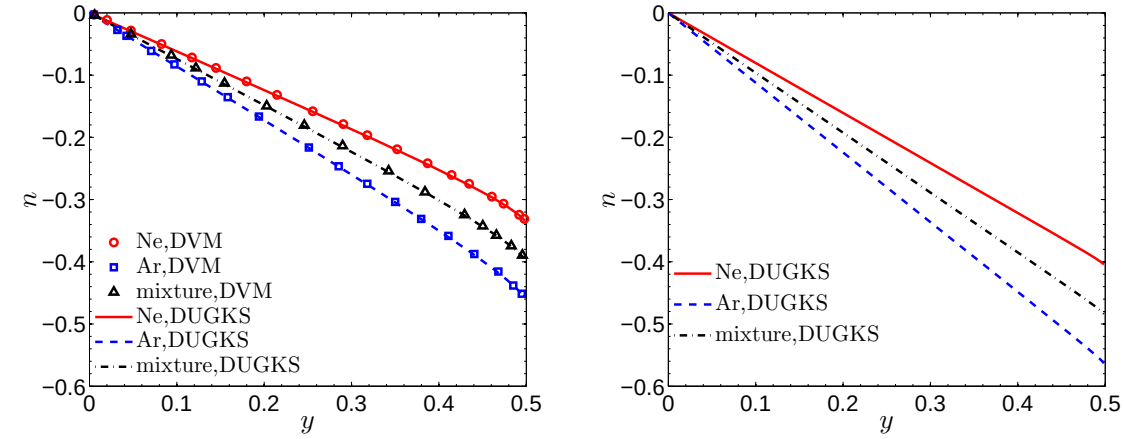

(c) $\delta = 10$, $C_0 = 0.5$ (d) $\delta = 100$, $C_0 = 0.5$

FIG. 7: The number density in the Fourier flow for the Ne-Ar mixture with $C_0 = 0.5$.

and 8. Good agreement can be found between the DUGKS and the DVM based on the McCormack model[27] under both small and large mass ratios, respectively, as $\delta = 0.1$, 1, and 10. Moreover, the DUGKS results at $\delta = 100$ are displayed in Figs. 7(d) and 8(d). It is clear that differences in number densities of Ne and Ar near the hot wall increase with δ. Besides, the influence of the molar concentration C_0 on the number density has also been displayed in Table IV. The relative differences in the number density of Ne, Ar, and the mixture between the two numerical methods all increase with δ for all considered values of C_0 and the maximum difference of them is less than 0.5%. When the rarefaction parameter δ is fixed, the number density of each species increases with the molar concentration C_0,

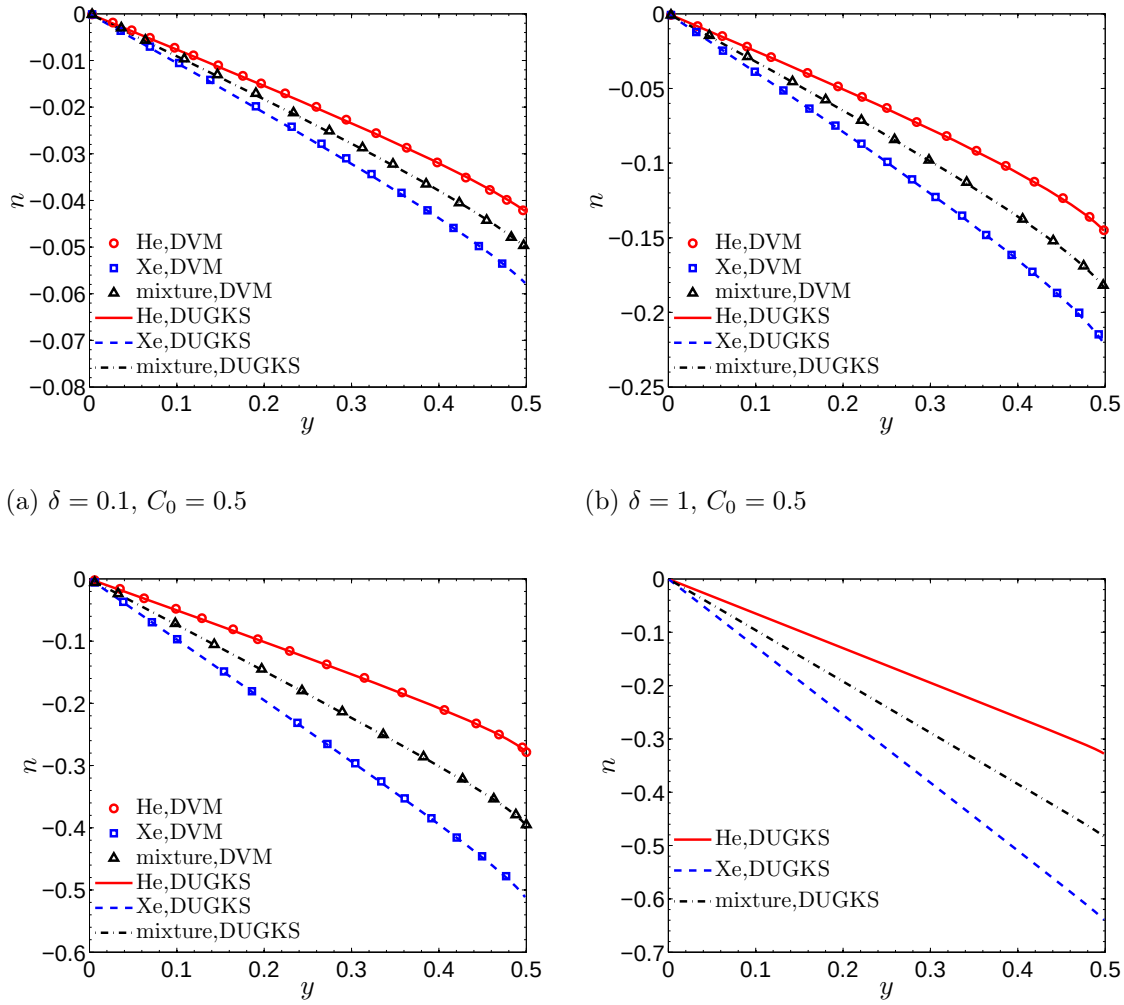

(a) $\delta = 0.1$, $C_0 = 0.5$

(b) $\delta = 1$, $C_0 = 0.5$

(c) $\delta = 10$, $C_0 = 0.5$

(d) $\delta = 100$, $C_0 = 0.5$

FIG. 8: The number density in the Fourier flow for the He-Xe mixture with $C_0 = 0.5$.

while that for the mixture varies slightly.

Figures 9 and 10 show the temperature variation of the Ne-Ar and He-Xe mixtures with $C_0 = 0.5$ as $\delta = 0.1$, 1, 10, and 100. It can be seen that the proposed DUGKS results agree well with those of the DVM based on the McCormack model[27]. The DUGKS results in Figs. 9(d) and 10(d) show that differences in temperature between species turn to vanish for $\delta = 100$. The influence of the molar concentration C_0 on the temperature of each species and the mixture is investigated in Table V. Similar with that of the number density, the maximum relative differences between the temperature of Ne, Ar, and the mixture from the two kinetic schemes is no more than 0.2% for all considered values of C_0 as $\delta = 0.1$, 1, and

TABLE IV: The number density n_{Ne}, n_{Ar}, and mixture velocity n at $y = H/2$ for the Ne-Ar mixture with different C_0 and δ.

δ	$-n_{Ne}$		$-n_{Ar}$		$-n$	
	Present	Ho et al.[27]	Present	Ho et al.[27]	Present	Ho et al.[27]
			$C_0 = 0.1$			
0.1	0.0482	0.0481	0.0577	0.0576	0.0568	0.0566
1	0.1576	0.1577	0.1946	0.1947	0.1909	0.1910
10	0.3079	0.3093	0.4073	0.4094	0.3974	0.3993
100	0.3710	—	0.4990	—	0.4862	—
1000	0.3929	—	0.5102	—	0.4985	—
			$C_0 = 0.5$			
0.1	0.0508	0.0507	0.0624	0.0624	0.0566	0.0566
1	0.1681	0.1680	0.2160	0.2159	0.1921	0.1920
10	0.3373	0.3375	0.4624	0.4631	0.3998	0.4003
100	0.4066	—	0.5660	—	0.4863	—
1000	0.4251	—	0.5717	—	0.4984	—
			$C_0 = 0.9$			
0.1	0.0552	0.0551	0.0705	0.0705	0.0567	0.0566
1	0.1846	0.1847	0.2494	0.2496	0.1911	0.1912
10	0.3808	0.3826	0.5474	0.5508	0.3974	0.3994
100	0.4649	—	0.6780	—	0.4862	—
1000	0.4815	—	0.6510	—	0.4985	—

10. Once the rarefaction parameter δ is fixed, the temperature of each species increases with the molar concentration C_0, while that for the mixture has small change. Besides, it is clear that the temperature of species and mixtures vary slightly as δ increases from 100 to 1000 under all values of C_0. The analytical solution of temperature variation[25] is available for $\delta = 1000$ and listed in the 3rd, 5th, and 7th columns of Table V as $\delta = 1000$ and C_0 varies from 0.1 to 0.9. It can be seen that the DUGKS result agrees well with the benchmark solution of the Navier-Stokes equations.

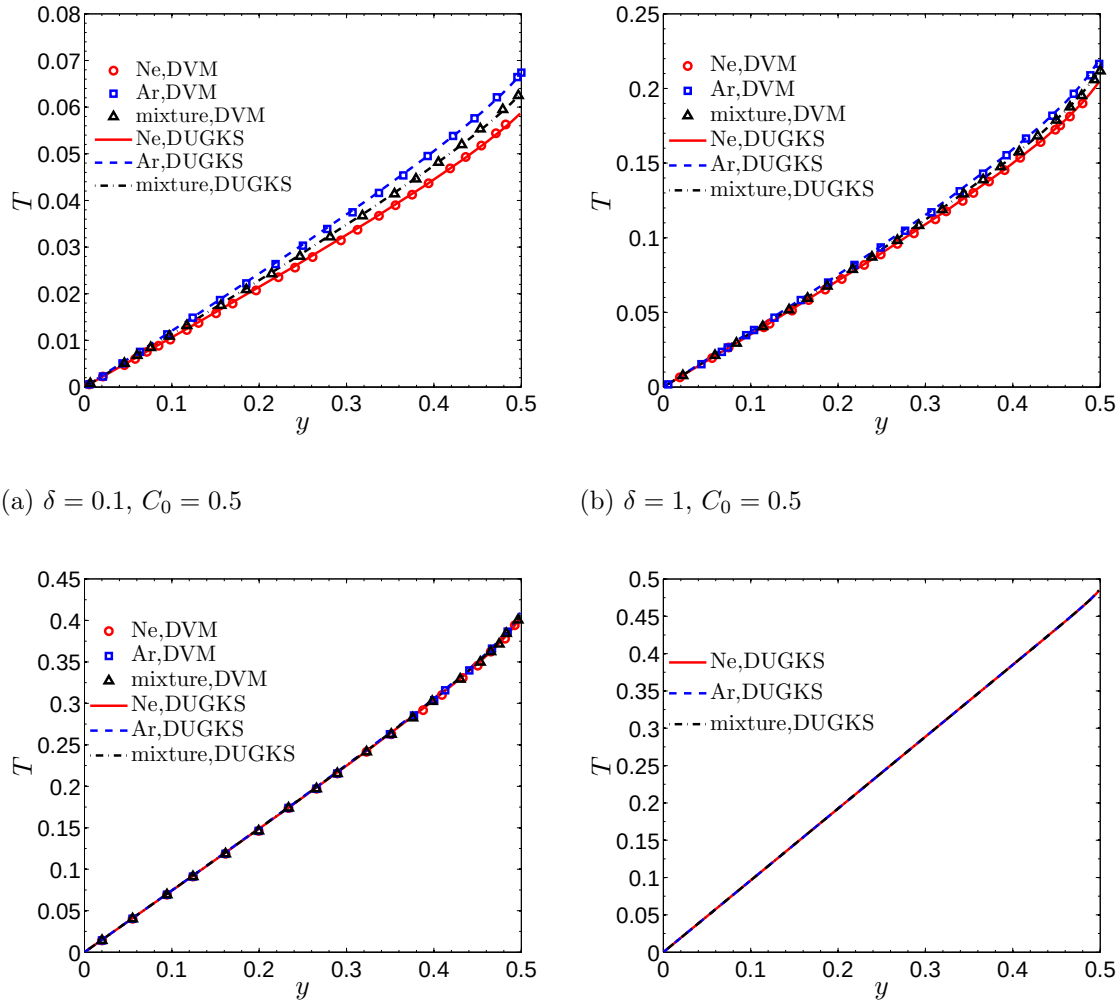

(a) $\delta = 0.1$, $C_0 = 0.5$

(b) $\delta = 1$, $C_0 = 0.5$

(c) $\delta = 10$, $C_0 = 0.5$

(d) $\delta = 100$, $C_0 = 0.5$

FIG. 9: Temperature profiles in the Fourier flow for the Ne-Ar mixture with $C_0 = 0.5$.

In Fig. 11, the molar concentration C of the Ne-Ar and He-Xe mixtures, which is defined as the deviated concentration of the light species from its equilibrium value, are shown and compared with the results from the DVM[27,64]. Due to the thermodiffusion, the light species mainly concentrate on the hot plate, whereas the heavy species concentrate on the cold plate[65]. Again the results predicted by the present DUGKS are in close agreement with those of the DVM. Furthermore, the DUGKS also gives the results for $\delta = 100$, which show that differences of the molar concentration C of the Ne-Ar and He-Xe mixtures increase with δ.

The variation of heat flux q_y in the Ne-Ar and He-Xe mixtures are presented in Table VI

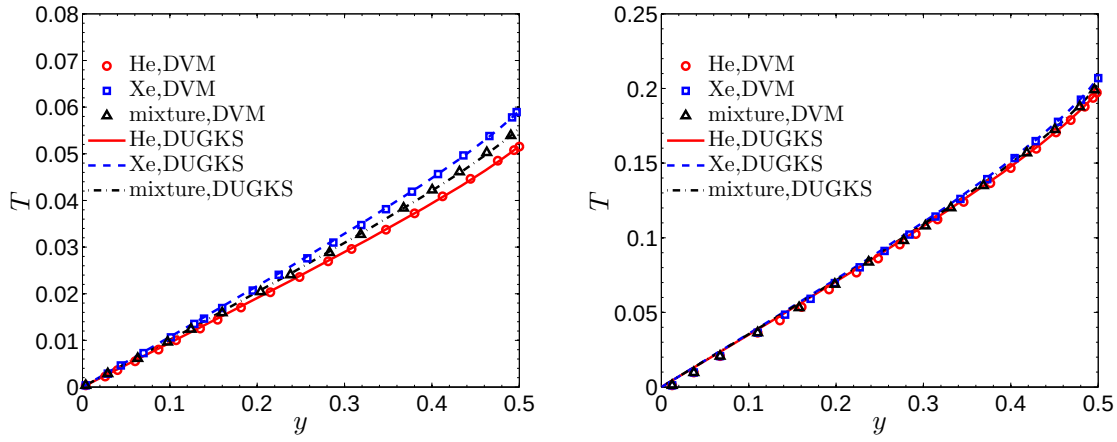

(a) $\delta = 0.1$, $C_0 = 0.5$ (b) $\delta = 1$, $C_0 = 0.5$

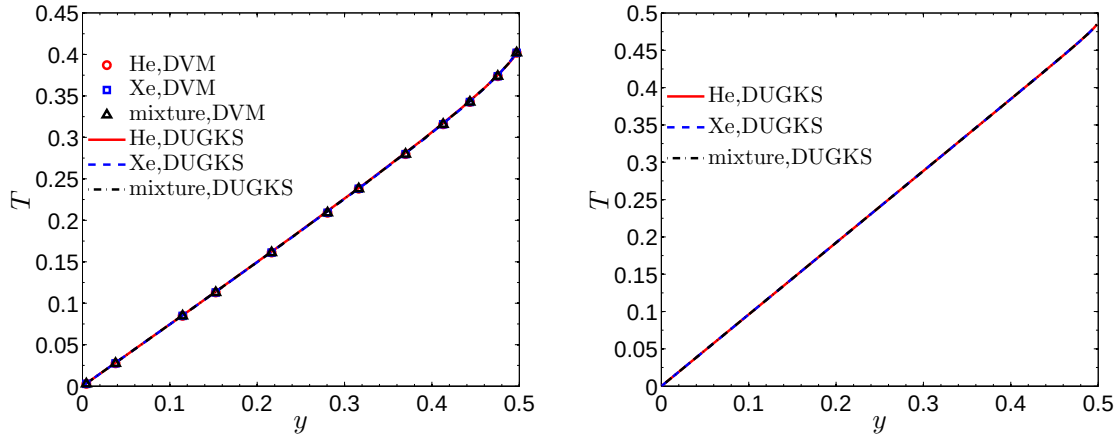

(c) $\delta = 10$, $C_0 = 0.5$ (d) $\delta = 100$, $C_0 = 0.5$

FIG. 10: Temperature profiles in the Fourier flow for the He-Xe mixture with $C_0 = 0.5$.

with varying mole fraction of the light species C_0 in each mixture for $\delta = 0.1$, 1, 10, 100, and 1000. From the data reported in Table VI, it is clear that the heat flux q_y decreases with the increasing rarefaction parameter δ for all considered C_0. Besides, for a fixed rarefaction parameter δ, the heat flux q_y turns to increase at first and then decrease with the increasing C_0 and the maximum value of q_y can be found at $C_0 = 0.5$. The results of the DUGKS and the DVM based on the McCormack model are nearly identical for both small and large mass ratios as $\delta = 0.1$, 1, and 10. In the case of $\delta = 1000$, the analytical solution of heat flux is included for comparisons in the 3rd, 5th, and 7th columns of Table VI for both the Ne-Ar

TABLE V: Species temperature T_{Ne} and T_{Ar} and mixture velocity T at $y = H/2$ for the Ne-Ar mixture with different C_0 and δ.

δ	T_{Ne}		T_{Ar}		T	
	Present	Ho et al.[27]	Present	Ho et al.[27]	Present	Ho et al.[27]
			$C_0 = 0.1$			
0.1	0.0570	0.0569	0.0641	0.0640	0.0634	0.0633
1	0.2020	0.2020	0.2135	0.2136	0.2124	0.2124
10	0.4040	0.4045	0.4086	0.4093	0.4083	0.4088
100	0.4871	—	0.4877	—	0.4876	—
1000	0.4986	0.5	0.4987	0.5	0.4986	0.5
			$C_0 = 0.5$			
0.1	0.0590	0.0589	0.0673	0.0673	0.0632	0.0631
1	0.2057	0.2056	0.2207	0.2205	0.2132	0.2131
10	0.4071	0.4065	0.4132	0.4127	0.4401	0.4096
100	0.4876	—	0.4882	—	0.4878	—
1000	0.4985	0.5	0.4986	0.5	0.4986	0.5
			$C_0 = 0.9$			
0.1	0.0623	0.0622	0.0728	0.0727	0.0633	0.0632
1	0.2106	0.2106	0.2296	0.2296	0.2125	0.2125
10	0.4075	0.4081	0.4148	0.4154	0.4083	0.4088
100	0.4875	—	0.4885	—	0.4876	—
1000	0.4986	0.5	0.4987	0.5	0.4986	0.5

and He-Xe mixtures. The solution of heat flux in hydrodynamic limit is given as[25]

$$q = \frac{m\kappa}{2k_B\mu}, \tag{52}$$

where κ is the heat conductivity of the mixture[66]. Results show that the DUGKS can accurately capture flow behaviors in the continuum regime.

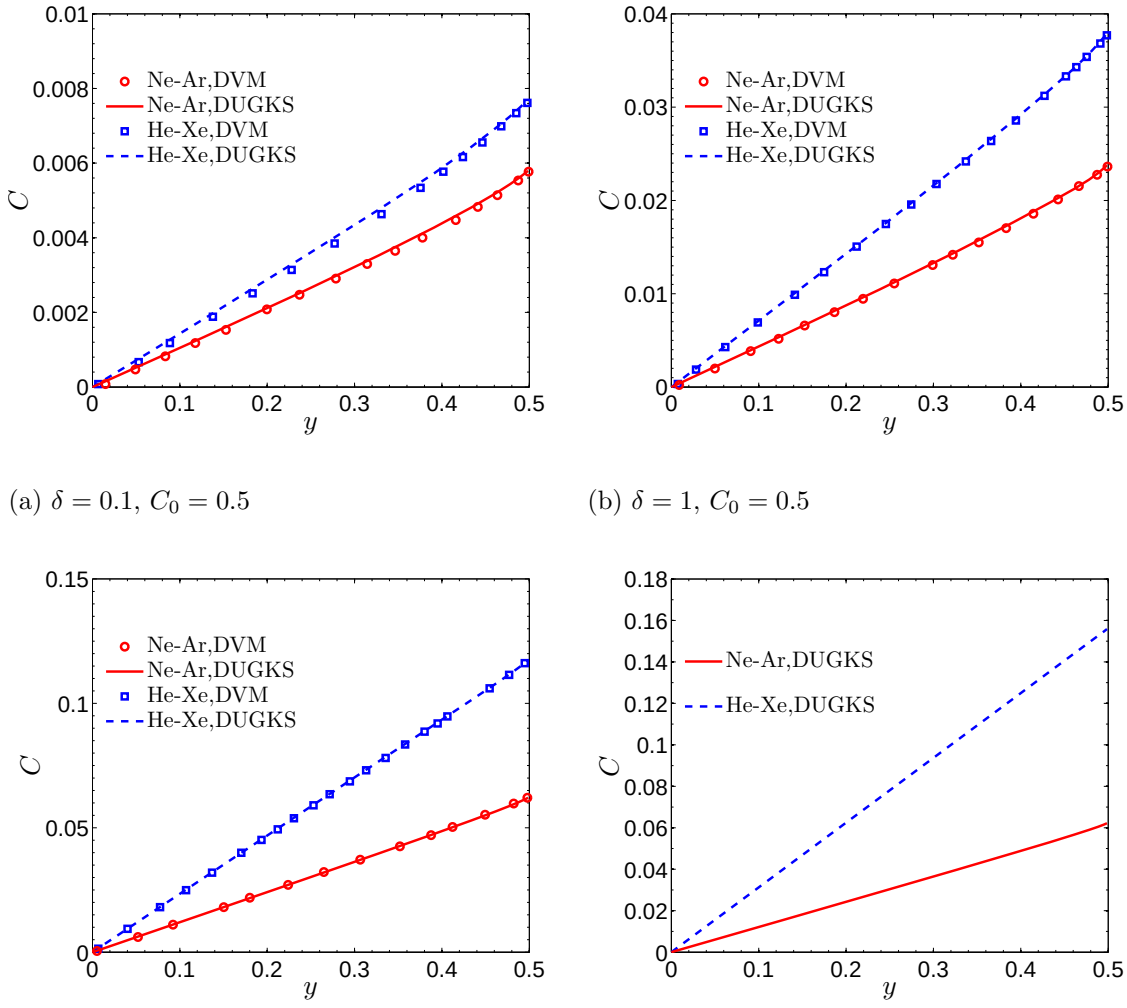

(a) $\delta = 0.1$, $C_0 = 0.5$

(b) $\delta = 1$, $C_0 = 0.5$

(c) $\delta = 10$, $C_0 = 0.5$

(d) $\delta = 100$, $C_0 = 0.5$

FIG. 11: Concentration of the light species in the Fourier flow for the Ne-Ar and He-Xe mixtures with $C_0 = 0.5$.

C. Lid-driven cavity flow

We now test the two-dimensional lid-driven cavity flow of binary gas mixtures. The flow domain considered is a two-dimensional square cavity with the length of walls being H in the Cartesian coordinate system (x, y). The upper wall located at $y = +H/2$ moves along the x direction at velocity U_w, which is much smaller than the characteristic molecular velocity v_0, while the other three (located at $x = \pm H/2$, $y = -H/2$) are fixed. The temperature of all the walls are kept at T_0, and they are fully diffusive. In this case, the boundary conditions

TABLE VI: The heat flux q_y in the Fourier flow of the Ne-Ar and He-Xe mixtures with different C_0 and δ.

δ	$C_0 = 0.1$		$C_0 = 0.5$		$C_0 = 0.9$	
	Present	Sharipov et al.[25]	Present	Sharipov et al.[25]	Present	Sharipov et al.[25]
			Ne-Ar			
0.1	0.5429	0.5430	0.5588	0.5588	0.5444	0.5445
1	0.4057	0.4058	0.4171	0.4172	0.4068	0.4069
10	0.1363	0.1364	0.1396	0.1397	0.1367	0.1368
100	0.01822	—	0.01864	—	0.01828	—
1000	0.00188	0.00189	0.00193	0.00194	0.00189	0.00190
			He-Xe			
0.1	0.7501	0.7500	1.3011	1.3011	1.0145	1.0145
1	0.5580	0.5582	0.9837	0.9839	0.7882	0.7883
10	0.1834	0.1834	0.03293	0.03303	0.2873	0.2875
100	0.02431	—	0.04436	—	0.04029	—
1000	0.00255	0.00252	0.00461	0.00461	0.00423	0.00422

have the following forms,

$$n_\alpha(x = \pm H/2) = \pm\frac{2}{\sqrt{\pi}}\int g_\alpha^{(in)}(x = \pm H/2)\exp(-c_{\alpha x}^2 - c_{\alpha y}^2)c_{\alpha x}dc_{\alpha x}dc_{\alpha y}, \tag{53a}$$

$$g_\alpha^{(out)}(x = \pm H/2) = (1 - a_\alpha)g_\alpha^{(in)}(x = \pm H/2) + a_\alpha n_\alpha(x = \pm H/2), \tag{53b}$$

$$\theta_\alpha^{(out)}(x = \pm H/2) = 0, \tag{53c}$$

$$n_\alpha(y = \pm H/2) = \pm\frac{2}{\sqrt{\pi}}\int g_\alpha^{(in)}(y = \pm H/2)\exp(-c_{\alpha x}^2 - c_{\alpha y}^2)c_{\alpha y}dc_{\alpha x}dc_{\alpha y}, \tag{53d}$$

$$g_\alpha^{(out)}(y = -H/2) = (1 - a_\alpha)g_\alpha^{(in)}(y = -H/2) + a_\alpha n_\alpha(y = -H/2), \tag{53e}$$

$$g_\alpha^{(out)}(y = +H/2) = (1 - a_\alpha)g_\alpha^{(in)}(y = +H/2) + a_\alpha\left[n_\alpha(y = +H/2) + 2\sqrt{\frac{m_\alpha}{m}}c_{\alpha x}\right], \tag{53f}$$

$$\theta_\alpha^{(out)}(y = \pm H/2) = 0. \tag{53g}$$

We also simulate this problem using the DSMC[67] to validate the proposed DUGKS. In this case, we focus on the velocity profiles of the mixtures. The DSMC is a stochastic particle-based method, where macroscopic quantities are obtained by averaging appropriate

microscopic properties of the simulated molecules. Therefore, the simulated results exhibits statistical noise due to finite sampling in the presence of thermal fluctuations. According to the equilibrium statistical mechanics, the "noise-to-signal" ratio E_u in the estimate of the fluid velocity can be written as[68]

$$E_u = \frac{1}{Ma\sqrt{\gamma M N_0}}, \tag{54}$$

where Ma is the Mach number of the DSMC simulations, M is the number of sampling steps, and N_0 is the average number of simulated molecules in each cell. With our configurations ($Ma = 0.01$ and $N_0 = 100$), to achieve smoother velocity profiles, the error is set to be $E_u = 0.05\%$, for which about $M = 2.4 \times 10^8$ independent samples are needed. The physical space is divided into a uniform grid with 60×60 cells, whose results show very slight difference with those on a refined grid with 100×100 cells. As $\delta = 100$, the mesh size of the DUGKS is about 1.9 times of the mean free path for this case. The velocity space of each species is discretized by the Newton-Cotes quadrature with 101×101 velocity points distributed uniformly in $[-4, 4]\times[-4, 4]$ for $\delta = 0.1$, 1, and 10. The half-range Gauss-Hermite quadrature[58] is employed for $\delta = 100$ with 28×28 velocity points. The CFL number is 0.5 for all the cases.

The velocity profiles across the cavity center of the Ne-Ar and He-Xe mixtures with $C_0 = 0.5$ and $\delta = 0.1$, 1, 10, and 100 (Kn = 8.86, 0.886, 0.0886, and 0.00886 correspondingly) are shown in Figs. 12 and 13. Results predicted by the present DUGKS are in close agreement with those of the DSMC for both the Ne-Ar and He-Xe mixtures as δ varies from 0.1 to 100, except for the He-Xe mixture at $\delta = 10$, where some deviations can be found in the velocity in the x direction along the vertical center line of the cavity in comparison with that of the DSMC.

Besides, in order to evaluate the computational efficiency, the CPU time and numbers of iteration of the DUGKS and the DSMC under the same computational mesh are measured and displayed in Table VII. The DUGKS code runs with 24 cores to reach the steady state defined in Eq. (40). The DSMC[67] runs with the MPI using 24 cores to reach the noise state defined in Eq. (54). It is clear that the DUGKS is significantly faster than the DSMC for this problem.

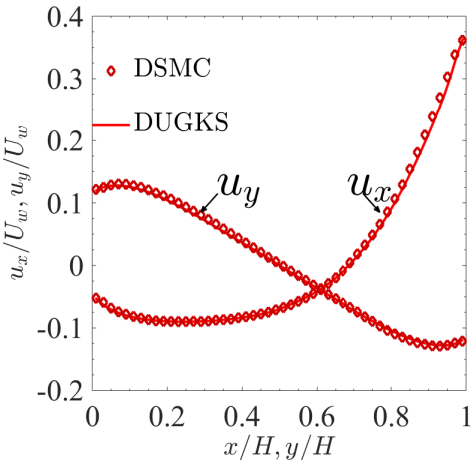

(a) $\delta = 0.1$, $C_0 = 0.5$

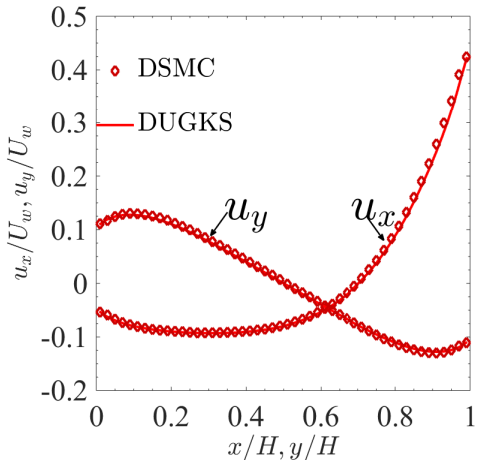

(b) $\delta = 1$, $C_0 = 0.5$

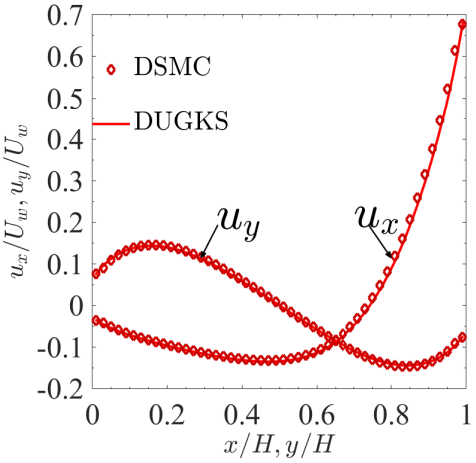

(c) $\delta = 10$, $C_0 = 0.5$

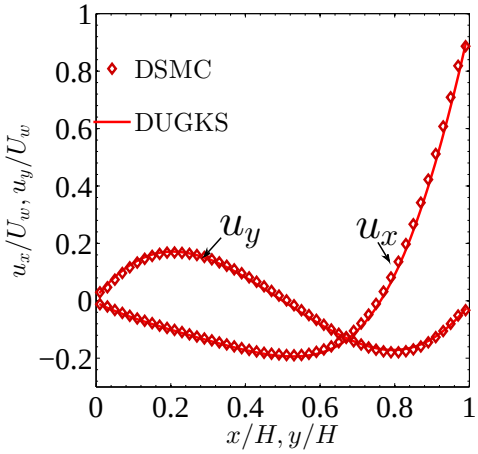

(d) $\delta = 100$, $C_0 = 0.5$

FIG. 12: Velocity profiles along the center lines in the cavity flow for the Ne-Ar mixture with $C_0 = 0.5$.

V. CONCLUSIONS

In this paper, a discrete unified gas kinetic scheme for binary gas mixtures has been developed for binary gas mixtures on the basis of the McCormack model, which can recover all the correct transport coefficients accurately. With the intrinsic coupling of molecular collision and transport processes in determining of the flux across the cell interface, the computational time step and mesh size are not limited by the mean collision time and mean free path of gas molecules, respectively, so that the multiscale flow physics of gas mixtures

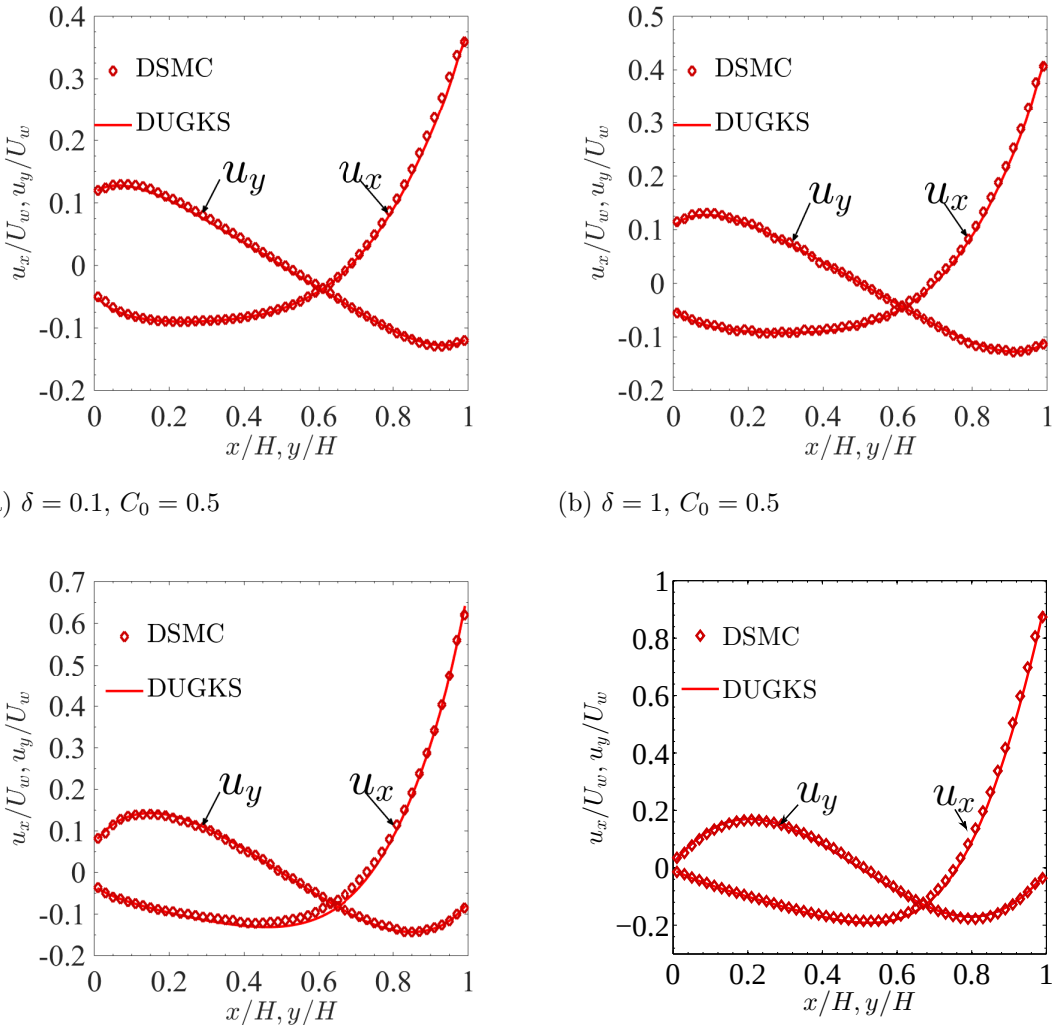

(a) $\delta = 0.1$, $C_0 = 0.5$

(b) $\delta = 1$, $C_0 = 0.5$

(c) $\delta = 10$, $C_0 = 0.5$

(d) $\delta = 100$, $C_0 = 0.5$

FIG. 13: Velocity profiles along the center lines in the cavity flow for the He-Xe mixture with $C_0 = 0.5$.

can be efficiently and self-adaptively captured from the hydrodynamic to the free-molecular flow regimes.

The proposed method is validated by several problems, including the Couette flow, the Fourier flow, and the lid-driven cavity flow for Ne-Ar and He-Xe mixtures. For the Couette and Fourier flows ranging from near-continuum to free molecular regimes, good agreement can be observed from the results of the DUGKS and the DVM based on the McCormack model for both small and large mass ratios. As for the 2D lid-driven cavity flow, the DUGKS results agree well with those of the DSMC. In addition, the DUGKS is more than

TABLE VII: Wall time (in seconds) and iteration steps of reaching steady states. 24 cores are employed by the DUGKS and the DSMC.

δ	Ne-Ar				He-Xe			
	DUGKS		DSMC		DUGKS		DSMC	
	time	step	time	step	time	step	time	step
0.1	4313	7432	1,634,891	2.4×10^8	6522	10077	1,527,409	2.4×10^8
1	3102	4525	1,666,654	2.4×10^8	8476	14215	1,541,555	2.4×10^8
10	4692	7277	1,672,260	2.4×10^8	10000	18031	1,562,775	2.4×10^8
100	1738	29925	1,816,130	2.4×10^8	5035	109316	1,655,976	2.4×10^8

two orders of magnitude faster than the DSMC for low-speed flows in terms of the wall time and convergent iteration steps. The presented results about classical test problems are essential to convince the audience that DUGKS is a good scheme for numerically solving the McCormack model.

Note that compared to most of the other kinetic models, the McCormack model can reproduce all transport kinetic coefficients, which ensures the reliability of this model equation. Comparisons have been performed between the AAP model and the McCormack model for simulating Couette flows over a wide range of the rarefaction parameter. Numerical results show that the McCormack model approximates the LBE and the full Boltzmann equation better than the AAP model in the transitional and near-continuum regimes for large mass ratio cases. However, the McCormack model can only be applied to the flows that slightly deviate from equilibrium, and is therefore unsuitable for nonlinear problems. In the future work, more advanced kinetic models for binary gas mixtures, such as the recently proposed BGK-type models[69,70], will be employed by the DUGKS to get further insights into the kinetic models for mixtures and study nonlinear problems in all the flow regimes.

ACKNOWLEDGMENTS

This study is financially supported by the National Natural Science Foundation of China (No. 11872024).

Appendix A: Macroscopic quantities solving for the 2D problem

We take the 2D Fourier flow as an example to show how to calculate the macroscopic quantities [see Eq. (24)] needed at the cell center and interface using the moments of the distribution functions $\tilde{\phi}_\alpha$ and $\bar{\phi}_\alpha$, respectively. For this problem, the isotropy in the xz plane is considered in Eqs. (A3) and (A4), i.e.,

$$P_{\alpha xx} = P_{\alpha zz}. \tag{A1}$$

Besides, the stress tensor $P_{\alpha ik}(\alpha = A, B; i, k = x, y, z)$ is traceless, which can be expressed as

$$P_{\alpha xx} + P_{\alpha yy} + P_{\alpha zz} = 0. \tag{A2}$$

Thus the terms G_α and Θ_α in Eqs. (22) and (23) have the following forms according to Eq. (A1) and (A2)

$$\begin{aligned}
G_\alpha =&\gamma_\alpha n_\alpha + 2\sqrt{\frac{m_\alpha}{m}}\left[\gamma_\alpha u_{\alpha x} - \nu^{(1)}_{\alpha\beta}(u_{\alpha x} - u_{\beta x}) - \nu^{(2)}_{\alpha\beta}(q_{\alpha x} - \frac{m_\alpha}{m_\beta}q_{\beta x})\right] c_{\alpha x} \\
&+ 2\sqrt{\frac{m_\alpha}{m}}\left[\gamma_\alpha u_{\alpha y} - \nu^{(1)}_{\alpha\beta}(u_{\alpha y} - u_{\beta y}) - \nu^{(2)}_{\alpha\beta}(q_{\alpha y} - \frac{m_\alpha}{m_\beta}q_{\beta y})\right] c_{\alpha y} \\
&+ \left[\gamma_\alpha T_\alpha - 2\frac{m_{\alpha\beta}}{m_\beta}(T_\alpha - T_\beta)\nu^{(1)}_{\alpha\beta}\right]\left(c^2_{\alpha x} + c^2_{\alpha y} - 1\right) \\
&+ 4\left[(\gamma_\alpha - \nu^{(3)}_{\alpha\alpha} + \nu^{(4)}_{\alpha\alpha} + \nu^{(3)}_{\alpha\beta})P_{\alpha xy} + \nu^{(4)}_{\alpha\beta}P_{\beta xy}\right] c_{\alpha x}c_{\alpha y} \\
&+ 2\left[(\gamma_\alpha - \nu^{(3)}_{\alpha\alpha} + \nu^{(4)}_{\alpha\alpha} + \nu^{(3)}_{\alpha\beta})P_{\alpha yy} + \nu^{(4)}_{\alpha\beta}P_{\beta yy}\right]\left(c^2_{\alpha y} - \frac{1}{2}c^2_{\alpha x} - \frac{1}{4}\right) \\
&+ \frac{8}{5}\sqrt{\frac{m_\alpha}{m}}\left[(\gamma_\alpha - \nu^{(5)}_{\alpha\alpha} + \nu^{(6)}_{\alpha\alpha} - \nu^{(5)}_{\alpha\beta})q_{\alpha x} + \nu^{(6)}_{\alpha\beta}\sqrt{\frac{m_\beta}{m_\alpha}}q_{\beta x} - \frac{5}{8}\nu^{(2)}_{\alpha\beta}(u_{\alpha x} - u_{\beta x})\right] c_{\alpha x}\left(c^2_{\alpha x} + c^2_{\alpha y} - 2\right) \\
&+ \frac{8}{5}\sqrt{\frac{m_\alpha}{m}}\left[(\gamma_\alpha - \nu^{(5)}_{\alpha\alpha} + \nu^{(6)}_{\alpha\alpha} - \nu^{(5)}_{\alpha\beta})q_{\alpha y} + \nu^{(6)}_{\alpha\beta}\sqrt{\frac{m_\beta}{m_\alpha}}q_{\beta y} - \frac{5}{8}\nu^{(2)}_{\alpha\beta}(u_{\alpha y} - u_{\beta y})\right] c_{\alpha y}\left(c^2_{\alpha x} + c^2_{\alpha y} - 2\right),
\end{aligned} \tag{A3}$$

and

$$\begin{aligned}
\Theta_\alpha =&\frac{1}{2}\left[\gamma_\alpha T_\alpha - 2\frac{m_{\alpha\beta}}{m_\beta}(T_\alpha - T_\beta)\nu^{(1)}_{\alpha\beta}\right] - \frac{1}{2}\left[(\gamma_\alpha - \nu^{(3)}_{\alpha\alpha} + \nu^{(4)}_{\alpha\alpha} + \nu^{(3)}_{\alpha\beta})P_{\alpha yy} + \nu^{(4)}_{\alpha\beta}P_{\beta yy}\right] \\
&+ \frac{4}{5}\sqrt{\frac{m_\alpha}{m}}\left[(\gamma_\alpha - \nu^{(5)}_{\alpha\alpha} + \nu^{(6)}_{\alpha\alpha} - \nu^{(5)}_{\alpha\beta})q_{\alpha x} + \nu^{(6)}_{\alpha\beta}\sqrt{\frac{m_\beta}{m_\alpha}}q_{\beta x} - \frac{5}{8}\nu^{(2)}_{\alpha\beta}(u_{\alpha x} - u_{\beta x})\right] c_{\alpha x} \\
&+ \frac{4}{5}\sqrt{\frac{m_\alpha}{m}}\left[(\gamma_\alpha - \nu^{(5)}_{\alpha\alpha} + \nu^{(6)}_{\alpha\alpha} - \nu^{(5)}_{\alpha\beta})q_{\alpha y} + \nu^{(6)}_{\alpha\beta}\sqrt{\frac{m_\beta}{m_\alpha}}q_{\beta y} - \frac{5}{8}\nu^{(2)}_{\alpha\beta}(u_{\alpha y} - u_{\beta y})\right] c_{\alpha y}.
\end{aligned} \tag{A4}$$

Then the moments of the linear term G_α can be given as

$$\int G_\alpha f_\alpha^r d\boldsymbol{c}_\alpha = \gamma_\alpha n_\alpha, \tag{A5a}$$

$$\int c_{\alpha i} G_\alpha f_\alpha^r d\boldsymbol{c}_\alpha = \gamma_\alpha u_{\alpha i} - \nu_{\alpha\beta}^{(1)}\left(u_{\alpha i} - u_{\beta i}\right) - \nu_{\alpha\beta}^{(2)}\left(q_{\alpha i} - \sqrt{\frac{m_\alpha}{m_\beta}} q_{\beta i}\right), \tag{A5b}$$

$$\int c_{\alpha x} c_{\alpha y} G_\alpha f_\alpha^r d\boldsymbol{c}_\alpha = \left[\left(\gamma_\alpha - \nu_{\alpha\alpha}^{(3)} + \nu_{\alpha\alpha}^{(4)} - \nu_{\alpha\beta}^{(3)}\right)\right] P_{\alpha xy} + \nu_{\alpha\beta}^{(4)} P_{\beta xy}, \tag{A5c}$$

$$\begin{aligned}&\int \left(c_{\alpha y}^2 + c_{\alpha x}^2 - 1\right) G_\alpha f_\alpha^r d\boldsymbol{c}_\alpha \\ &= \frac{1}{2}\left[\left(\gamma_\alpha - \nu_{\alpha\alpha}^{(3)} + \nu_{\alpha\alpha}^{(4)} - \nu_{\alpha\beta}^{(3)}\right) P_{\alpha yy} + \nu_{\alpha\beta}^{(4)} P_{\beta yy}\right] + \left[\gamma_\alpha T_\alpha - 2\frac{m_{\alpha\beta}}{m_\beta}\left(T_\alpha - T_\beta\right)\nu_{\alpha\beta}^{(1)}\right],\end{aligned} \tag{A5d}$$

$$\begin{aligned}&\int \left(2c_{\alpha y}^2 - c_{\alpha x}^2 - \frac{1}{2}\right) G_\alpha f_\alpha^r d\boldsymbol{c}_\alpha \\ &= \frac{5}{2}\left[\left(\gamma_\alpha - \nu_{\alpha\alpha}^{(3)} + \nu_{\alpha\alpha}^{(4)} - \nu_{\alpha\beta}^{(3)}\right) P_{\alpha yy} + \nu_{\alpha\beta}^{(4)} P_{\beta yy}\right] + \frac{1}{2}\left[\gamma_\alpha T_\alpha - 2\frac{m_{\alpha\beta}}{m_\beta}\left(T_\alpha - T_\beta\right)\nu_{\alpha\beta}^{(1)}\right],\end{aligned} \tag{A5e}$$

$$\begin{aligned}&\int c_{\alpha i}\left(c_{\alpha y}^2 + c_{\alpha x}^2 - 2\right) G_\alpha f_\alpha^r d\boldsymbol{c}_\alpha \\ &= \frac{8}{5}\sqrt{\frac{m_\alpha}{m}}\left[\left(\gamma_\alpha - \nu_{\alpha\alpha}^{(5)} + \nu_{\alpha\alpha}^{(6)} - \nu_{\alpha\beta}^{(5)}\right) q_{\alpha i} + \nu_{\alpha\beta}^{(6)} q_{\beta i} - \frac{5}{8}\nu_{\alpha\beta}^{(2)}\left(u_{\alpha i} - u_{\beta i}\right)\right],\end{aligned} \tag{A5f}$$

where $f_\alpha^r = \pi^{-1}\exp\left(-c_{\alpha x}^2 - c_{\alpha y}^2\right)$, $i = x, y$, and $\alpha, \beta = A, B$. In addition, the moments of Θ_α have the following forms,

$$\begin{aligned}&\int \Theta_\alpha f_\alpha^r d\boldsymbol{c}_\alpha \\ &= -\frac{1}{2}\left[\left(\gamma_\alpha - \nu_{\alpha\alpha}^{(3)} + \nu_{\alpha\alpha}^{(4)} - \nu_{\alpha\beta}^{(3)}\right) P_{\alpha yy} + \nu_{\alpha\beta}^{(4)} P_{\beta yy}\right] + \frac{1}{2}\left[\gamma_\alpha T_\alpha - 2\frac{m_{\alpha\beta}}{m_\beta}\left(T_\alpha - T_\beta\right)\nu_{\alpha\beta}^{(1)}\right],\end{aligned} \tag{A6a}$$

$$\int c_{\alpha i}\Theta_\alpha f_\alpha^r d\boldsymbol{c}_\alpha = \frac{2}{5}\sqrt{\frac{m_\alpha}{m}}\left[\left(\gamma_\alpha - \nu_{\alpha\alpha}^{(5)} + \nu_{\alpha\alpha}^{(6)} - \nu_{\alpha\beta}^{(5)}\right) q_{\alpha i} + \nu_{\alpha\beta}^{(6)} q_{\beta i} - \frac{5}{8}\nu_{\alpha\beta}^{(2)}\left(u_{\alpha i} - u_{\beta i}\right)\right], \tag{A6b}$$

Next, according to Eq. (30), the moments of the of distribution functions $\tilde{g}_\alpha$ and $\tilde{\theta}_\alpha$ can

be obtained as

$$\int \tilde{g}_\alpha f_\alpha^r d\boldsymbol{c}_\alpha = n_\alpha, \tag{A7a}$$

$$\int c_{\alpha i}\tilde{g}_\alpha f_\alpha^r d\boldsymbol{c}_\alpha = u_{\alpha i} + \frac{\Delta t}{2}\omega_\alpha \left[\nu_{\alpha\beta}^{(1)}\left(u_{\alpha i} - u_{\beta i}\right) + \nu_{\alpha\beta}^{(2)}\left(q_{\alpha i} - \sqrt{\frac{m_\alpha}{m_\beta}}q_{\beta i}\right)\right], \tag{A7b}$$

$$\int c_{\alpha x}c_{\alpha y}\tilde{g}_\alpha f_\alpha^r d\boldsymbol{c}_\alpha = \left[1 + \frac{\Delta t}{2}\omega_\alpha\left(\nu_{\alpha\alpha}^{(3)} - \nu_{\alpha\alpha}^{(4)} + \nu_{\alpha\beta}^{(3)}\right)\right] P_{\alpha xy} - \frac{\Delta t}{2}\omega_\alpha \nu_{\alpha\beta}^{(4)} P_{\beta xy}, \tag{A7c}$$

$$\frac{2}{3}\int \left[\left(c_{\alpha y}^2 + c_{\alpha x}^2 - 1\right)\tilde{g}_\alpha + \tilde{\theta}_\alpha\right] f_\alpha^r d\boldsymbol{c}_\alpha = T_\alpha + \Delta t\omega_\alpha \frac{m_{\alpha\beta}}{m_\beta}\left(T_\alpha - T_\beta\right)\nu_{\alpha\beta}^{(1)}, \tag{A7d}$$

$$\begin{aligned}\frac{1}{3}\int &\left[\left(2c_{\alpha y}^2 - c_{\alpha x}^2 - \frac{1}{2}\right)\tilde{g}_\alpha - \tilde{\theta}_\alpha\right] f_\alpha^r d\boldsymbol{c}_\alpha \\ &= \left[1 + \frac{\Delta t}{2}\omega_\alpha\left(\nu_{\alpha\alpha}^{(3)} - \nu_{\alpha\alpha}^{(4)} + \nu_{\alpha\beta}^{(3)}\right)\right] P_{\alpha yy} - \frac{\Delta t}{2}\omega_\alpha \nu_{\alpha\beta}^{(4)} P_{\beta yy},\end{aligned} \tag{A7e}$$

$$\begin{aligned}\frac{1}{2}\int &c_{\alpha i}\left[\left(c_{\alpha y}^2 + c_{\alpha x}^2 - 2\right)\tilde{g}_\alpha + \tilde{\theta}_\alpha\right] f_\alpha^r d\boldsymbol{c}_\alpha \\ &= \sqrt{\frac{m_\alpha}{m}}\left[q_{\alpha i} + \frac{\Delta t}{2}\omega_\alpha\left(\nu_{\alpha\alpha}^{(5)} - \nu_{\alpha\alpha}^{(6)} + \nu_{\alpha\beta}^{(5)}\right)q_{\alpha i} - \frac{\Delta t}{2}\nu_{\alpha\beta}^{(6)} q_{\beta i} + \frac{5\Delta t}{16}\omega_\alpha \nu_{\alpha\beta}^{(2)}\left(u_{\alpha i} - u_{\beta i}\right)\right].\end{aligned} \tag{A7f}$$

Once the distribution functions $\tilde{g}_\alpha$ and $\tilde{\theta}_\alpha$ are known, the number density n_α of species α can be calculated from Eq. (A7a). The velocity u_{Ai}, u_{Bi} and heat flux q_{Ai}, q_{Bi} can be obtained from solving the linear equation set consisted by Eqs. (A7b) and (A7f) for $\alpha, \beta = A, B$. The macroscopic quantities P_{Axy} and P_{Bxy} can be calculated from the linear equation set consisted by Eq. (A7c) for $\alpha, \beta = A, B$. Similarly, the macroscopic quantities P_{Ayy} and P_{Byy} and T_A and T_B can be solved from Eqs. (A7e) and (A7d), respectively.

At last, the moments of the distribution functions $\bar{g}_\alpha$ and $\bar{\theta}_\alpha$ have the same expressions with those of the distribution functions $\tilde{g}_\alpha$ and $\tilde{\theta}_\alpha$, except that the term Δt in Eq. (A7) is replaced by $\Delta t/2$ due to the definition of $\bar{g}_\alpha$ and $\bar{\theta}_\alpha$ according to Eq. (33). Similarly, the macroscopic quantities on the interface at half time step can be solved from the moments of $\bar{g}_\alpha$ and $\bar{\theta}_\alpha$.

REFERENCES

[1]F. Sharipov, *Rarefied gas dynamics: fundamentals for research and practice* (John Wiley & Sons, 2015).

[2]G. A. Bird, *Molecular Gas Dynamics and the Direct Simulation of Gas Flows* (Clarendon Press, 1994).

[3]D. Bruno, M. Capitelli, and S. Longo, "Dsmc modelling of vibrational and chemical kinetics for a reacting gas mixture," Chemical physics letters **289**, 141–149 (1998).

[4]F. Sharipov and J. L. Strapasson, "Benchmark problems for mixtures of rarefied gases. I. Couette flow," Physics of Fluids **25**, 027101.

[5]J. L. Strapasson and F. Sharipov, "Ab initio simulation of heat transfer through a mixture of rarefied gases," International Journal of Heat and Mass Transfer **71**, 91–97 (2014).

[6]F. Sharipov, "Ab initio simulation of gaseous mixture flow through an orifice," Vacuum **143**, 106–118 (2017).

[7]J. Fan and C. Shen, "Statistical Simulation of Low-Speed Rarefied Gas Flows," Journal of Computational Physics **167**, 393–412 (2001).

[8]L. L. Baker and N. G. Hadjiconstantinou, "Variance reduction for Monte Carlo solutions of the Boltzmann equation," Physics of Fluids **17**, 051703 (2005).

[9]T. M. M. Homolle and N. G. Hadjiconstantinou, "A low-variance deviational simulation Monte Carlo for the Boltzmann equation," Journal of Computational Physics **226**, 2341–2358 (2007).

[10]L. Szalmas, "Variance-reduced DSMC for binary gas flows as defined by the McCormack kinetic model," Journal of Computational Physics **231**, 3723–3738 (2012).

[11]S. Kosuge, K. Aoki, and S. Takata, "Shock-wave structure for a binary gas mixture: finite-difference analysis of the Boltzmann equation for hard-sphere molecules," European Journal of Mechanics-B/Fluids **20**, 87–126 (2001).

[12]S. Takata, S. Yasuda, S. Kosuge, and K. Aoki, "Numerical analysis of thermal-slip and diffusion-slip flows of a binary mixture of hard-sphere molecular gases," Physics of Fluids **15**, 3745–3766 (2003).

[13]R. Garcia and C. Siewert, "The viscous-slip, diffusion-slip, and thermal-creep problems for a binary mixture of rigid spheres described by the linearized Boltzmann equation," European Journal of Mechanics-B/Fluids **26**, 749–778 (2007).

[14]R. D. M. Garcia and C. E. Siewert, "The linearized Boltzmann equation with Cercignani-cLampis boundary conditions: Basic flow problems in a plane channel," European Journal of Mechanics - B/Fluids **28**, 387–396 (2009).

[15]L. Wu, J. Zhang, J. M. Reese, and Y. Zhang, "A fast spectral method for the boltzmann equation for monatomic gas mixtures," Journal of Computational Physics **298**, 602–621 (2015).

[16]P. L. Bhatnagar, E. P. Gross, and M. Krook, "A model for collision processes in gases. I. Small amplitude processes in charged and neutral one-component systems," Phys. Rev. **94**, 511–525 (1954).

[17]P. Andries, K. Aoki, and B. Perthame, "A consistent BGK-type model for gas mixtures," Journal of Statistical Physics **106**, 993–1018 (2002).

[18]M. Groppi, S. Monica, and G. Spiga, "A kinetic ellipsoidal BGK model for a binary gas mixture," EPL (Europhysics Letters) **96**, 64002 (2011).

[19]S. Brull, V. Pavan, and J. Schneider, "Derivation of a BGK model for mixtures," European Journal of Mechanics-B/Fluids **33**, 74–86 (2012).

[20]M. Bisi and S. Lorenzani, "High-frequency sound wave propagation in binary gas mixtures flowing through microchannels," Physics of Fluids **28**, 052003 (2016).

[21]F. J. McCormack, "Construction of linearized kinetic models for gaseous mixtures and molecular gases," The Physics of Fluids **16**, 2095–2105 (1973).

[22]F. Sharipov, L. M. G. Cumin, and D. Kalempa, "Plane Couette flow of binary gaseous mixture in the whole range of the Knudsen number," European Journal of Mechanics-B/Fluids **23**, 899–906 (2004).

[23]S. Naris, D. Valougeorgis, D. Kalempa, and F. Sharipov, "Flow of gaseous mixtures through rectangular microchannels driven by pressure, temperature, and concentration gradients," Physics of fluids **17**, 100607 (2005).

[24]S. Takata, H. Sugimoto, and S. Kosuge, "Gas separation by means of the Knudsen compressor," European Journal of Mechanics-B/Fluids **26**, 155–181 (2007).

[25]F. Sharipov, L. M. G. Cumin, and D. Kalempa, "Heat flux between parallel plates through a binary gaseous mixture over the whole range of the Knudsen number," Physica A: Statistical Mechanics and its Applications **378**, 183–193 (2007).

[26]L. Szalmas, J. Pitakarnnop, S. Geoffroy, S. Colin, and D. Valougeorgis, "Comparative study between computational and experimental results for binary rarefied gas flows through long microchannels," Microfluidics and nanofluidics **9**, 1103–1114 (2010).

[27]M. T. Ho, L. Wu, I. Graur, Y. Zhang, and J. M. Reese, "Comparative study of the Boltzmann and McCormack equations for Couette and Fourier flows of binary gaseous mixtures," International Journal of Heat and Mass Transfer **96**, 29–41 (2016).

[28]P. Asinari and L.-S. Luo, "A consistent lattice Boltzmann equation with baroclinic coupling for mixtures," Journal of Computational Physics **227**, 3878–3895 (2008).

[29]Z. Guo, P. Asinari, and C. Zheng, "Lattice Boltzmann equation for microscale gas flows of binary mixtures," Physics Review E **79**, 026702 (2009).

[30]S. Naris, D. Valougeorgis, F. Sharipov, and D. Kalempa, "Discrete velocity modelling of gaseous mixture flows in MEMS," Superlattices and Microstructures **35**, 629–643 (2004).

[31]D. Valougeorgis and S. Naris, "Acceleration schemes of the discrete velocity method: Gaseous flows in rectangular microchannels," SIAM Journal on Scientific Computing **25**, 534–552 (2003).

[32]R. Garcia and C. Siewert, "Channel flow of a binary mixture of rigid spheres described by the linearized Boltzmann equation and driven by temperature, pressure, and concentration gradients," SIAM Journal on Applied Mathematics **67**, 1041–1063 (2007).

[33]R. Garcia and C. Siewert, "Couette flow of a binary mixture of rigid-sphere gases described by the linearized Boltzmann equation," European Journal of Mechanics-B/Fluids **27**, 823–836 (2008).

[34]R. Wang and K. Xu, "Unified gas-kinetic scheme for multi-species non-equilibrium flow," in *AIP Conference Proceedings*, Vol. 1628 (AIP, 2014) pp. 970–975.

[35]R. Wang, *Unified gas-kinetic scheme for the study of non-equilibrium flows*, Ph.D. thesis, Hong Kong University of Science and Technology (2015).

[36]Z. Guo, K. Xu, and R. Wang, "Discrete unified gas kinetic scheme for all Knudsen number flows: Low-speed isothermal case," Physics Review E **88**, 033305 (2013).

[37]Z. Guo, R. Wang, and K. Xu, "Discrete unified gas kinetic scheme for all Knudsen number flows. II. Thermal compressible case," Physics Review E **91**, 033313 (2015).

[38]K. Xu and J.-C. Huang, "A unified gas-kinetic scheme for continuum and rarefied flows," Journal of Computational Physics **229**, 7747–7764 (2010).

[39]J.-C. Huang, K. Xu, and P. Yu, "A unified gas-kinetic scheme for continuum and rarefied flows II: multi-dimensional cases," Communications in Computational Physics **12**, 662–690 (2012).

[40]P. Wang, L.-P. Wang, and Z. Guo, "Comparison of the lattice Boltzmann equation and discrete unified gas-kinetic scheme methods for direct numerical simulation of decaying turbulent flows," Physical Review E **94**, 043304 (2016).

[41]P. Wang, Y. Zhang, and Z. Guo, "Numerical study of three-dimensional natural convection in a cubical cavity at high Rayleigh numbers," International Journal of Heat and Mass Transfer **113**, 217–228 (2017).

[42]L. Zhu, Z. Guo, and K. Xu, "Discrete unified gas kinetic scheme on unstructured meshes," Computers & Fluids **127**, 211–225 (2016).

[43]L. Zhu and Z. Guo, "Application of discrete unified gas kinetic scheme to thermally induced nonequilibrium flows," Computers & Fluids (2017), 10.1016/j.compfluid.2017.09.019.

[44]Z. Guo and K. Xu, "Discrete unified gas kinetic scheme for multiscale heat transfer based on the phonon Boltzmann transport equation," International Journal of Heat and Mass Transfer **102**, 944–958 (2016).

[45]C. Zhang, K. Yang, and Z. Guo, "A discrete unified gas-kinetic scheme for immiscible two-phase flows," International Journal of Heat and Mass Transfer **126**, 1326–1336 (2018).

[46]Y. Zhang, L. Zhu, R. Wang, and Z. Guo, "Discrete unified gas kinetic scheme for all Knudsen number flows. III. Binary gas mixtures of Maxwell molecules," Physical Review E **97**, 053306 (2018).

[47]G. M. Kremer, *An introduction to the Boltzmann equation and transport processes in gases* (Springer Science & Business Media, 2010).

[48]S. Chapman, T. G. Cowling, and D. Burnett, *The mathematical theory of non-uniform gases: an account of the kinetic theory of viscosity, thermal conduction and diffusion in gases* (Cambridge university press, 1970).

[49]E. Shakhov, "Generalization of the Krook kinetic relaxation equation," Fluid Dynamics **3**, 95–96 (1968).

[50]F. Sharipov and D. Kalempa, "Gaseous mixture flow through a long tube at arbitrary Knudsen numbers," Journal of Vacuum Science & Technology A: Vacuum, Surfaces, and Films **20**, 814–822 (2002).

[51]C. Chu, "Kinetic-theoretic description of the formation of a shock wave," The Physics of Fluids **8**, 12–22 (1965).

[52]J. Yang and J. Huang, "Rarefied flow computations using nonlinear model Boltzmann equations," Journal of Computational Physics **120**, 323–339 (1995).

[53]B. Van Leer, "Towards the ultimate conservative difference scheme. IV. A new approach to numerical convection," Journal of computational physics **23**, 276–299 (1977).

[54]L. Mieussens, "On the asymptotic preserving property of the unified gas kinetic scheme for the diffusion limit of linear kinetic models," Journal of Computational Physics **253**, 138–156 (2013).

[55]L. Zhu, P. Wang, and Z. Guo, "Performance evaluation of the general characteristics

based off-lattice boltzmann scheme and DUGKS for low speed continuum flows," Journal of Computational Physics **333**, 227–246 (2017).

[56]C. Wu, B. Shi, Z. Chai, and P. Wang, "Discrete unified gas kinetic scheme with a force term for incompressible fluid flows," Computers & Mathematics with Applications **71**, 2608–2629 (2016).

[57]F. Sharipov and V. Seleznev, "Data on internal rarefied gas flows," Journal of Physical and Chemical Reference Data **27**, 657–706 (1998).

[58]B. Shizgal, "A Gaussian quadrature procedure for use in the solution of the Boltzmann equation and related problems," Journal of Computational Physics **41**, 309–328 (1981).

[59]L. Wu, J. M. Reese, and Y. Zhang, "Solving the Boltzmann equation deterministically by the fast spectral method: application to gas microflows," Journal of Fluid Mechanics **746**, 53–84 (2014).

[60]J. Iannacci, M. Huhn, C. Tschoban, and H. Pötter, "Rf-mems technology for future mobile and high-frequency applications: reconfigurable 8-bit power attenuator tested up to 110 ghz," IEEE Electron Device Letters **37**, 1646–1649 (2016).

[61]L. Yang, C. Shu, J. Wu, and Y. Wang, "Numerical simulation of flows from free molecular regime to continuum regime by a dvm with streaming and collision processes," Journal of Computational Physics **306**, 291–310 (2016).

[62]L. Yang, C. Shu, W. Yang, Z. Chen, and H. Dong, "An improved discrete velocity method (DVM) for efficient simulation of flows in all flow regimes," Physics of Fluids **30**, 062005 (2018).

[63]P. Wang, M. T. Ho, L. Wu, Z. Guo, and Y. Zhang, "A comparative study of discrete velocity methods for low-speed rarefied gas flows," Computers & Fluids **161**, 33–46 (2018).

[64]S. Srinivasan and M. Z. Saghir, *Thermodiffusion in Multicomponent Mixtures: Thermodynamic, Algebraic, and Neuro-Computing Models* (Springer Science & Business Media, 2012).

[65]R. Wang, X. Xu, K. Xu, and T. Qian, "Onsager's cross coupling effects in gas flows confined to micro-channels," Physical Review Fluids **1**, 044102 (2016).

[66]F. Sharipov and D. Kalempa, "Velocity slip and temperature jump coefficients for gaseous mixtures. iv. Temperature jump coefficient," International Journal of Heat and Mass Transfer **48**, 1076–1083 (2005).

[67]T. Scanlon, E. Roohi, C. White, M. Darbandi, and J. Reese, "An open source, parallel

DSMC code for rarefied gas flows in arbitrary geometries," Computers & Fluids **39**, 2078–2089 (2010).

[68]N. G. Hadjiconstantinou, A. L. Garcia, M. Z. Bazant, and G. He, "Statistical error in particle simulations of hydrodynamic phenomena," Journal of computational physics **187**, 274–297 (2003).

[69]J. R. Haack, C. D. Hauck, and M. S. Murillo, "A conservative, entropic multispecies BGK model," Journal of Statistical Physics **168**, 826–856 (2017).

[70]A. V. Bobylev, M. Bisi, M. Groppi, G. Spiga, and I. F. Potapenko, "A general consistent BGK model for gas mixtures." Kinetic & Related Models **11** (2018), 10.3934/krm.2018054.